Universidade de Aveiro
2022

Daniel Tiago Rebelo de Andrade

Técnicas de Gestão de Feixe de onda para sistemas Massive MIMO nas redes 5G NR

Beam Management Techniques for Massive MIMO systems in 5G NR networks

Universidade de Aveiro
2022

Daniel Tiago Rebelo de Andrade

Técnicas de Gestão de Feixe de onda para sistemas Massive MIMO nas redes 5G NR

Beam Management Techniques for Massive MIMO systems in 5G NR networks

Dissertação apresentada à Universidade de Aveiro para cumprimento dos requisitos necessários à obtenção do grau de Mestre em Engenharia Eletrónica e Telecomunicações, realizada sob a orientação científica do Professor Doutor Adão Paulo Soares da Silva (orientador), Professor Associado do Departamento de Eletrónica, Telecomunicações e Informática da Universidade de Aveiro e do Doutor Roberto Magueta (coorientador), investigador da Allbesmart LDA.

O júri / The jury

Presidente / President

Doutor Telmo Reis Cunha
Professor Associado da Universidade de Aveiro

Vogais / Examiners committee

Doutora Gordana-Raluca Barb
Professora Auxiliar, Facultatea de Electronica, Telecomunicatii Si Tehnologii Informationale Politehnica University, Timisoara

Doutor Adão Paulo Soares da Silva
Professor Associado da Universidade de Aveiro (Orientador)

Agradecimentos/ Acknowledgments

Quero agradecer ao Professor Doutor Adão Silva (orientador) e ao Doutor Roberto Magueta (coorientador) pelos ensinamentos transmitidos, compreensão, ajuda e constante disponibilidade ao longo da realização deste trabalho.

A todos os meus colegas de curso com quem fui convivendo, pela partilha de saberes e espírito de entreajuda que tanto foram úteis a ultrapassar quaisquer contratempos ao longo destes últimos anos.

A todos os meus amigos, pela sua presença em todos os momentos e paciência aquando da minha menor disponibilidade.

À minha família pela motivação e apoio incondicional, providenciando tudo o que precisei ao longo da minha vida.

E ainda a todos os que de forma direta ou indireta contribuíram para a realização desta dissertação.

Palavras-chave

5G, NR, 3GPP, MIMO Massivo, comunicações na banda das ondas milimétricas, modulação OFDM, camada PHY, RAN, técnica de formação de feixe, acesso inicial, gerenciamento de feixe

Resumo

O uso de frequências na banda das ondas milimétricas é visto como uma tecnologia chave para os futuros sistemas de comunicação móveis, tendo em vista a ultrapassar o problema da escassez de banda a sub-6 GHz, e por permitir as elevadas taxas de dados requeridas para sistemas 5G/6G. Contudo, a propagação deste tipo de ondas está associado a perdas acentuadas em espaço livre e várias atenuações que se tornam cada vez mais significativas com o aumento do valor da frequência, impondo obstáculos à comunicação.

Para ultrapassar estas adversidades, agregados constituídos por múltiplos elementos de antena são implementados por forma a permitir técnicas de formação de feixe e possibilitar a transmissão de feixes mais estreitos e altamente direcionais, diminuindo os níveis de interferência e melhorando consequentemente o link budget. Deste modo, para assegurar constantemente que a comunicação efetuada em cada dispositivo ocorre utilizando o conjunto de feixes que proporciona o melhor nível de conectividade, é então necessário um conjunto de procedimentos de controlo de gestão de feixe, assegurando um estabelecimento eficiente da comunicação e a sua contínua manutenção entre um dispositivo e a rede.

Esta dissertação descreve o procedimento de gestão de feixe conhecido como estabelecimento inicial de feixe, focando o processo de seleção do melhor par de feixe de transmissão-receção disponível após o uso de técnicas de varrimento de feixe por fim a efetuar medições dos diferentes níveis de potência do sinal recebido. O principal objetivo passa pela conceção de um novo algoritmo de estabelecimento de par de feixes baseado em estimações de ângulo (BSAE), que explora o uso de múltiplos SSBs definidos pelo 3GPP, por forma a maximizar o RSRP no recetor, através do feixe selecionado. Esta otimização é feita usando os sinais de sincronização secundários (SSSs) presentes em cada SSB para efetuar uma estimação de canal no domínio digital (que contém o efeito do processamento analógico). Depois, combinando essas estimações, foi feita uma estimação da matriz do canal de propagação, sem o efeito desse processamento analógico. Finalmente, através da matriz do canal de propagação, foi determinado o ângulo que maximiza o RSRP, e calculado o feixe através do vetor de resposta do agregado.

Os resultados obtidos demonstram que o algoritmo proposto atinge melhor desempenho quando comparado com o algoritmo convencional de seleção de par de feixes. Foi feita ainda uma comparação com o caso ótimo, isto é, com o caso em que se conhece completamente o canal e se obtém um angulo ótimo. Os resultados obtidos pelo algoritmo proposto foram muito próximos do caso ótimo, pelo que é bastante interessante para sistemas práticos 5G mmWave mMIMO, que estejam de acordo com o padrão 3GPP.

keywords

5G, NR, 3GPP, massive MIMO, millimeter-Wave communications, OFDM, PHY, RAN, Beamforming, Initial Access, Beam Management

abstract

The use of Millimeter wave (mmWave) spectrum frequencies is seen as a key enabler technology for the future wireless communication systems to overcome the bandwidth shortage of the sub 6GHz microwave spectrum band, enabling high speed data transmissions in the 5G/6G systems. Nevertheless, mmWave propagation characteristics are associated to significant free-path losses and many more attenuations that become even more harsher as the frequency increases, rendering the communication challenging at this frequencies.

To overcome these distinct disadvantages, multiple antenna arrays are employed to allow beamforming techniques for the transmission of narrower concentrated beams in more precise directions and less interference levels between them, consequently improving the link budget. Thus, to constantly assure that the communication with each device is done using the beam pair that allows the best possible connectivity, a set of Beam Management control procedures is necessary to assure an efficient beamformed connection establishment and its continuous maintenance between the device and the network.

This dissertation will address the description of the Initial Beam Establishment (IBE) BM procedure, focusing the selection of the most suitable transmit-receive beam pair available after completed beam sweeping techniques to measure the different power levels of the received signal. The main goal is to design a new 3GPP-standard compliant beam pair selection algorithm based on SSS angle estimation (BSAE), that makes use of multiple Synchronization Signal Blocks (SSBs) to maximize the Reference Signal Received Power (RSRP) value at the receiver, through the selected beam pair. This optimization is done using the Secondary Synchronization Signals (SSSs) present in each SSB to perform channel estimation in the digital domain (comprising the effects of the analog processing). Afterwards, the combination of those estimations were used to perform the equivalent channel propagation matrix estimation without the analog processing effects. Finally, through the channel propagation matrix, the angle that maximizes the RSRP was determined to compute the most suitable beam through the aggregated response vector.

The obtained results show that the proposed algorithm achieves better performance levels compared to a conventional beam pair selection algorithm. Furthermore, a comparison with an optimal case is also done, i.e., the situation where the channel is known, and the optimal beam pair angle can be determined. Therefore, the similar performance results compared to the optimal case indicates that the proposed algorithm is interesting for practical 5G mmWave mMIMO implementations, according to 3GPP-compliant standards.

Contents

List of Figures

List of Tables

List of Acronyms

1G	First Generation
2G	Second Generation
3G	Third Generation
3GPP	Third Generation Partnership Project
3GPP2	Third Generation Partnership Project 2
4G	Fourth Generation
5G	Fifth Generation
5GC	5G Core Network
5GS	5G System
AA	Antenna Array
AAS	Active Antenna System
ADC	Analog-to-Digital Conversion
AMC	Adaptative Modulation and Coding
AMPS	Advanced Mobile Phone System
AWGN	Additive White Gaussian Noise
BER	Bit Error Rate
BF	Beamforming
BM	Beam Management
BPSK	Binary Phase-Shift Keying
BS	Base Station
BW	Bandwidth
BWP	Bandwidth Part
CDMA	Code Division Multiple Access
CDMA2000	Code Division Multiple Access 2000
CP	Cyclic Prefix
CRB	Common Resource Blocks

CSI	Channel State Information
DAC	Digital-to-Analog Converter
D-AMPS	Digital-Advanced Mobile Phone System
DCCH	Dedicated Control Channel
DCI	Downlink Control Information
DL	Downlink
DL-SCH	Downlink Shared Channel
DM-RS	Demodulation Reference signal
DoF	Degrees of Freedom
EDGE	Enhanced Data Rate for Global Evolution
EHF	Extremely High Frequency
eMBB	Enhanced Mobile Broadband
FDD	Frequency Division Duplex
FDM	Frequency Division Multiplexing
FDMA	Frequency Division Multiple Access
FFT	Fast Fourier Transform
FM	Frequency Modulation
FR1	Frequency Range 1
FR2	Frequency Range 2
GMSK	Gaussian Minimum Shift Keying
gNB	Next Generation Node B
GP	Guard Period
GPRS	General Packet Radio Service
GPS	Global Positioning System
GSM	Global System for Mobile Communications
HARQ	Hybrid Automatic Request
HF	High Frequency
HSDPA	High-Speed Downlink Packet Access

HSUPA	High-Speed Uplink Packet Access
IA	Initial Access
IFFT	Inverse Fast Fourier Transform
IMT	International Mobile Telecommunications
INI	Inter Numerology Interference
IPTV	Internet Protocol Television
ISI	Inter-Symbol Interference
ITU	International Telecommunications Union
ITU-R	International Telecommunications Union-Radiocommunications Sector
L1	Layer 1
L2	Layer 2
LIDAR	Light Detection And Ranging
LoS	Line of Sight
LTE	Long-Term Evolution
MAC	Medium Access Control
MBB	Mobile Broadband
MIB	Master Information Block
MIMO	Multiple-Input Multiple-Output
mMIMO	Massive Multiple-Input Multiple-Output
MMS	Multimedia Message Service
mMTC	Massive Machine-Type Communication
mmW	Millimeter Wave
M-QAM	M-ary Quadrature Amplitude Modulation
MU-MIMO	Multi-User MIMO
NAS	Non-Access Stratum
ng-eNB	Next Generation Evolved Node B
NG-RAN	Next Generation Radio Access Network
NMT	Nordic Mobile Telephony

NR	New Radio
NSA	Non-Standalone
OFDM	Orthogonal Frequency Division Multiplexing
OFDMA	Orthogonal Frequency-Division Multiple Access
PAPR	Peak-to-Average Power Ratio
PBCH	Physical Broadcast Channel
PCI	Physical Cell Identity
PDC	Personal Digital Cellular
PDCCH	Physical Downlink Control Channel
PHY	Physical Layer
PRACH	Physical Random-Access Channel
PRB	Physical Resource Blocks
PSK	Phase-Shift Keying
PSS	Primary Synchronization Signal
PTRS	Phase-Tracking Reference Signal
QoS	Quality of Service
QPSK	Quadrature Phase-Shift Keying
RA	Random Access
RAN	Radio Access Network
RB	Resource Block
RF	Radio Frequency
RLC	Radio Link Control
RRC	Radio Resource Control
RSRP	Reference Signal Received Power
RX	Receiver
SA	Standalone
SC-FDMA	Single Carrier Frequency Division Multiple Access
SCS	Subcarrier Spacing

SI	System Information
SIB	System Information Block
SIB1	System Information Block 1
SINR	Signal-to-Interference plus Noise Ratio
SMS	Short Message Service
SNR	Signal-to-Noise Ratio
SRS	Sounding Reference Signal
SS	Synchronization Signal
SSB	Synchronization Signal Block
SSS	Secondary Synchronization Signal
TACS	Total Access Communication System
TB	Transport Block
TBS	Transport Block Size
TCP	Transport Control Protocol
TDD	Time Division Duplex
TDMA	Time-Division Multiple Access
TX	Transmitter
UE	User Equipment
UL	Uplink
ULA	Uniform Linear Array
UMTS	Universal Mobile Telecommunication System
UPA	Uniform Planar Array
URLLC	Ultra-Reliable Low Latency Communication
UTRA	Universal Terrestrial Radio Access
WAP	Wireless Application Protocol
W-CDMA	Wideband Code Division Multiple Access
WWW	World WideWeb

List of Symbols

Symbol	Description
$\tilde{d}_{k,s}$	Received SSS at the subcarrier *k* and analog beam *s*
$\triangle_{\emptyset}$	Angular range for the elevation
$\triangle_{f}$	Subcarrier Spacing
$\triangle_{\theta}$	Angular range for the azimuth
$\mathbf{H}_{k}$	Frequency domain channel matrix at the subcarrier *k*
$\mathbf{f}_{a}$	Analog vector modelling the analog beam at the BS
$\mathbf{h}_{a,\,k}$	Equivalent channel estimation in the analog part
$\mathbf{h}_{eq,\,k,\,s}$	Equivalent channel estimation in the digital part
$\mathbf{w}_{a,s}$	Analog vector modelling the *s*th analog beam at the UE
$BW_{Channel}$	Minimum channel bandwidth
N_{cl}	Number of clusters
N_{rx}	Number of receive antennas
N_{tx}	Number of transmit antennas
T_{SS}	SS Burst Periodicity
d_{k}	Transmitted SSS at the subcarrier *k*
f_{c}	Carrier centre frequency
f_{s}	Waveform sample rate
$\mathbf{n}_{k,s}$	Denotes the zero mean Gaussian noise, with variance σ_{n}^{2}
σ_{n}^{2}	Power of channel noise
L	Number of SSBs in a SS burst

N	Number of symbols
S	Number of beams in the beam sweeping procedure
s and k	Analog beam and subcarrier indices, respectively

Notation

Operator	**Description**
tr(.)	Trace of a matrix
$(.)^*$	Conjugate of a matrix
$(.)^T$	Transpose of a matrix
$(.)^H$	Hermitian of a matrix

Chapter 1

1. Introduction

This chapter begins with a brief description about the historical background of mobile communication systems which have been in permanent evolution, witnessing five distinct generations over the last 50 years. Then, an overview of the current under development 5G generation is presented to give a better understanding of the implemented work. After, the motivations and objectives are described, followed by the original contributions of this work. Lastly, the structure of this dissertation is presented.

1.1 Background and basic concepts of cellular communication systems

Telecommunications, particularly wireless mobile networks, have become an essential part in our societies since they are a revolutionized connectivity element that promotes the economic growth of countries all around the world while providing a conformation of the information society and current knowledge. In the last 50 years, the cellular communication systems evolution has generated new resources and services to the end users worldwide over distinct generations:

- **1G**

  The first generation of mobile communications (1G) appeared in 1980 and was limited to voice services over analog systems based on circuit-switching, frequency modulation (FM) and frequency division multiple access (FDMA) to allocate different frequency bands for all the users [1]. Some of the first 1G worldwide main technologies used were the Advanced Mobile Phone System (AMPS) standard, developed in North America, the Nordic Mobile Telephony (NMT), created in the Nordic countries and the Total Access Communication System (TACS), which was used in the United Kingdom. All these cellular systems made mobile telephony accessible to ordinary people for the first time but were also presented with innumerous drawbacks, such as has low-capacity unreliable handoff, poor quality untrustworthy voice links and also the impossibility to interoperate between countries due to the incompatibilities created by the different technologies at the time of their creation [2].

- **2G**

  The second generation of mobile communication (2G) emerged in the early 1990s to keep up with the demands originated by the exponential growth of the 1G. These new fully digital systems based on Time Division Multiple Access (TDMA), Frequency Division Duplex (FDD) and Gaussian Minimum Shift Keying (GMSK) modulation allowed innovative data services such as the Short Message Service (SMS), Multimedia Message Service (MMS) and improved

capacity, voice transmission quality and data rate [3]. Some of the numerous 2G technologies include both the Digital-AMPS (D-AMPS) and the Code Division Multiple Access (CDMA) used in the United States, the Personal Digital Cellular (PDC) used exclusively in Japan and the Global system for Mobile Communications (GSM) developed by many European Countries. The later GSM technology worldwide spread made it the most used standard globally, extending the success of the 1G generation, experienced by a small fraction of people, to a large majority of individuals, that still currently utilize 2G, preserving its importance nowadays [4].

The continuous improvement on the 2G technologies, alongside the creation of the World Wide Web (WWW) led to the appearance of some advance systems like the General Packet Radio Service (GPRS), on the informally known 2.5 generation (2.5G) and the later Enhanced Data Rate for global Evolution (EDGE), on the 2.75 generation (2.75G). The 2.5G GPRS technology introduced systems that had implemented an additional packet switched domain to the already existing circuit switched domain like the Transport Control Protocol (TCP) while enhancing the data rates supported by the 2G networks, providing some innovative services such as the Wireless Application Protocol (WAP) access and internet access. On the other hand, the 2.75G EDGE technology introduced the 8-Phase-Shift Keying (8PSK) encoding within existing GSM timeslots, allowing the achievement of higher data rates and more flexibility to carry both packet switch data and circuit switch data in comparison to GSM [1].

❖ 3G

The third generation of mobile communication (3G) appeared in the early 2000s to face once more the exponential growth of the mobile data services demand, requiring even higher data rates capable of enabling faster wireless internet access, a better Quality of service (QoS) and scalability [5]. Alongside all these innovations, it had also become apparent the need to surpass all the interoperability limitations of the different standards already adopted across different geographical locations, each one with its own regulatory issues, making the portability of the global roaming service impossible.

The plan of a new standard to overcome this lack of globalization while accommodating the backward compatibility of all the already existing networks, together with the definition of a common structure, under which all of them could evolve, was created by the International Telecommunication Union (ITU) and was named International Mobile Telephone 2000 (IMT-2000) standard. This standard had the intent to converge all the existent wireless systems in a global frequency band in the 2000 MHz range, supporting a single universal wireless communication standard across all the countries around the world.

As a result, two main systems emerged: the Universal Mobile Telecommunication System (UMTS) for Europe, based on GSM network with the main air interface know as Universal Terrestrial Radio Access (UTRA) with both Time division Duplex (TDD) and FDD modes and the Code Division Multiple Access 2000 (CDMA2000), used in the United States.

The evolution of these main systems towards 3G standardization, according the IMT-2000 specifications, was made by two organizational groups: The 3rd Generation Partnership Project (3GPP) [6], related to the based on Wideband Code Division Multiple Access (W-CDMA) evolved GSM networks and the associated radio access technologies supported, and the 3rd

Generation Partnership Project 2 (3GPP2), comprising North American and Asian interests developing global specifications for the CDMA2000 3G systems. These partnership projects unite several telecommunications standard development organizations and provide their members with a stable environment to produce technical specifications and technical reports for each of the two main 3G mobile systems standards, the European UMTS and the CDMA2000, mostly used in the United States.

These new 3G technologies enabled the efficient use of global roaming, service portability and multimedia, allowing the differentiation of products and wider range of more distinct and advanced services making use of the greater network capacity due to the enhanced spectral efficiency [7]. Some of these new applications over the previous networks included Global Positioning System (GPS) services, Internet Protocol Television (IPTV) support, wider area wireless voice services and improved audio and video streaming, among others [8].

As a similar way to the improvement process of the 2G technologies, so the 3G networks were also developed along the years to keep up with the market demands leading to the appearance of two newer technologies implemented in the 3G networks: the High-Speed Downlink Packet Access (HSDPA) on the informally know 3.5 generation (3.5G) and the High-speed Uplink Packet Access (HSUPA) on the 3.75 generation (3.75G).

The HSDPA is a W-CDMA packet-based data service protocol that allows faster Downlink (DL) data transmission speeds [9]. It has been implemented in some applications like fast cell search, Hybrid Automatic Repeat Request (HARQ), Adaptive Modulation and Coding (AMC), more advanced receiver (RX) designs and at Multiple-Input Multiple-Output (MIMO) systems. On the other hand, the HSUPA is a UMTS/WCDMA Uplink (UL) evolution technology complementary to the HSDPA, that enhances the UL data transmission speed [10].

❖ 4G

The fourth generation of mobile communications (4G), represented by the Long-Term Evolution (LTE) technology, was once more a response to a given demand, focused on a concept of inter-operability between different sorts of networks, being able to provide additional services and higher data transfer speeds. The LTE standard introduced the concept of division multiple access but in a different manner, this division is not done in time (TDMA) nor code (CDMA) but in a frequency domain equalization process at the DL known as Orthogonal Frequency-Division Multiple Access (OFDMA), enabling more advanced multi-antenna technologies as well as wider transmission BWs by providing orthogonality between the users, reducing the interference, and improving the network capacity [11]. On the other hand, LTE uses the technique of Single Carrier Frequency Division Multiple Access (SC-FDMA) at the UL, taking advantage of the lower Peak-to-Average Power Ratio (PAPR) to provide high spectral efficiency [12].

In comparison to 3G networks that supports mobile communication in unpaired spectrum using the TD-SCDMA radio access technology, the main difference is that LTE supports both FDD and TDD operations in just one radio access technology [13]. This new technology became responsible for the convergence of digital appliances and technologies into a unique mobile

communication technology used in almost all mobile-network operators, diminishing the data distribution boundaries related to both unpaired and paired spectra.

The Figure 1.1 shows the evolution of the already described mobile communications systems, along with their main associated technologies, from the 1G until 4G:

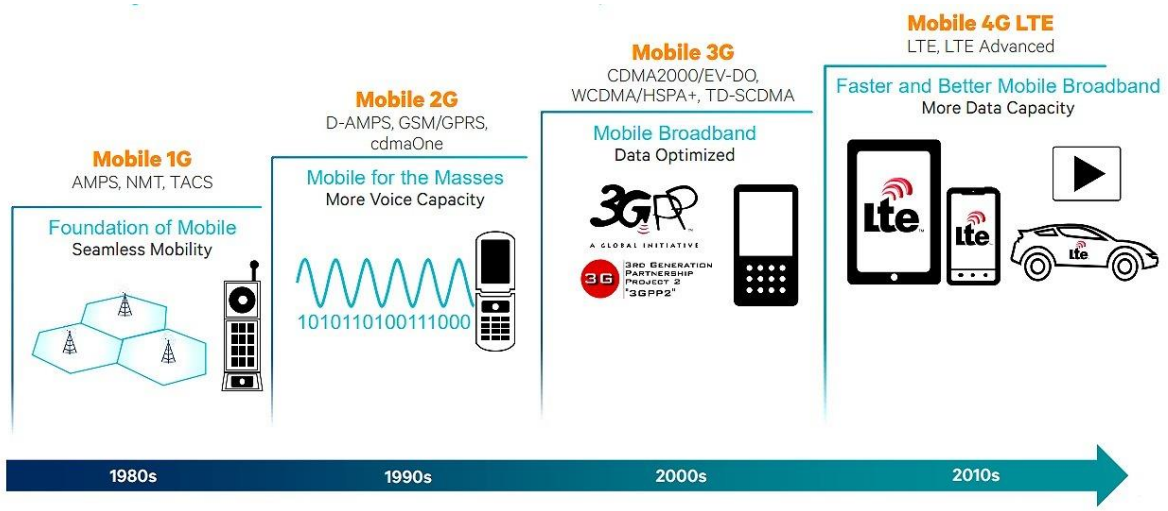

Figure 1.1: Mobile Communications systems evolution from 1G to 4G [14].

1.2 5G and the future of mobile communications

Even though LTE has proved to be a very capable technology, some requirements such as the lower latency levels to deliver more instantaneous and real-time communications were still not met. To answer this, the 3GPP organization, responsible to develop and maintain global technical specifications, initiated the development of the New Radio (NR) access technology. Discussions around the Fifth generation (5G) of mobile communication have been around for a while now, sometimes not only referring to the specific NR access technology but also to the new wide range of possibilities and services on the edge to be enabled by future mobile communication [15]. The new focus on providing not only connectivity between users but also between any device or application has a revolutionary impact in a wide range of different industries and services, such as the phone industry, automation, automotive industry, manufacturing, entertainment industries, health care and much more, providing to each of them new enhancements and opportunities with the main goal of improving the quality of life of all its users [16].

The radio communications sector of the International Telecommunications Union (ITU-R), responsible for ensuring efficient and economical use of the RF spectrum by all radio communication services, identified mainly three distinctive classes of 5G use cases to support the requirements of the International Mobile Telecommunications for 2020 (IMT-2020) standard, presented in Figure 1.2. These main use cases are Enhanced Mobile Broadband (eMBB), Massive Machine-Type Communication (mMTC) and Ultra-Reliable and Low Latency communication (URLLC) [17], [18]:

- **eMBB** corresponds to a response to the growing needs triggered by the evolution of mobile broadband (MBB) services offered by 4G, representing a wide range of scenarios from hot spots to wide-area coverage, allowing even larger data volumes and further enhanced user experience, for example, by supporting even higher end-user data rates, higher user densities, and the need for higher capacity levels [19].

- **mMTC** scenarios corresponds to pure machine-centric services typically characterized by a massive number of connected devices that consume and generate only a relatively small amount of non-delay sensitive data. The main requirements include low device cost and very low device energy consumption, allowing for very long device battery lifetime needed for subsequent remote deployment scenarios [20].

- **URLLC** scenarios are characterized by human and machine-centric communication services with strict requirements for very low latency, high reliability, and high availability. Examples hereof are vehicle-to-vehicle communication and remote medical surgeries [21].

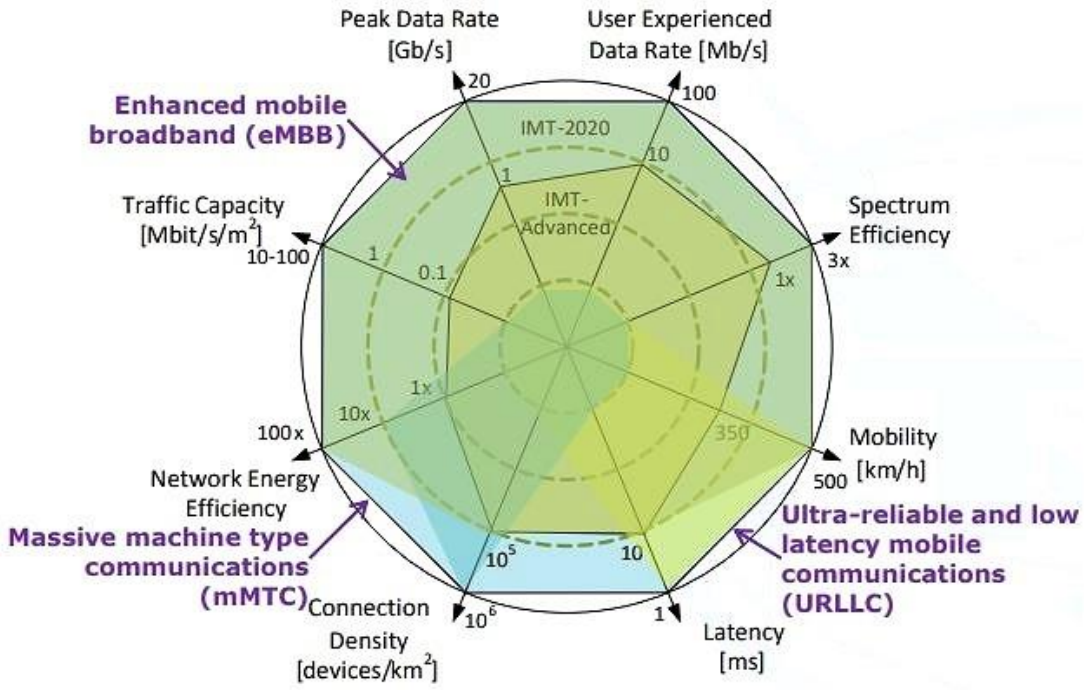

Figure 1.2: Three main use-cases and their key capabilities defined by ITU-R [22].

The initial set of NR specifications goes back to the concluded 3GPP Release 15, supporting both Non-Standalone (NSA) and Standalone (SA) network mode operation. The main difference between these two modes is that in NSA mode operation, 5G radio systems are integrated in previous LTE networks for coexistence and interworking assurance purposes, relying on them for initial access (IA) procedures and mobility while in SA mode, 5G NR systems are directly connected to a new developed 5G core network in conjunction with its own air interface.

By the end of 2018, as soon as the Release 15 work matured into the first full set of 5G standards in compliance with the first requirements towards the IMT-2020 standard, 3GPP started to shift its attention to the development of Release 16, the second installment of the global 5G standard, greatly expanding the reach of 5G to new services, spectrum, and deployments [23].

In the middle of 2020, with the completion of the Release 16, 3GPP continued the standardization work, expanding 5G into new devices, applications, and deployments, concluding the stage 3 of Release 17 in March of 2022. This current release marks the conclusion of the first phase of the 5G technology evolution and delivers additional enhancements to 5G systems at many levels, including capacity, coverage, latency, power, mobility, and many more improvements [24].

Meanwhile, new discussions about the recently approved Release 18 are being made towards the development of the 5G advanced era, beginning the second phase of the 5G technology developments in order to bring a new wave of wireless technology expansions to address the short and longer terms needs of a wide variety of new verticals and use cases across 5G systems, powered by artificial intelligence and extended reality technologies [25].

A representation of the main enhancements of the last mentioned 3GPP Releases is presented below in Figure 1.3:

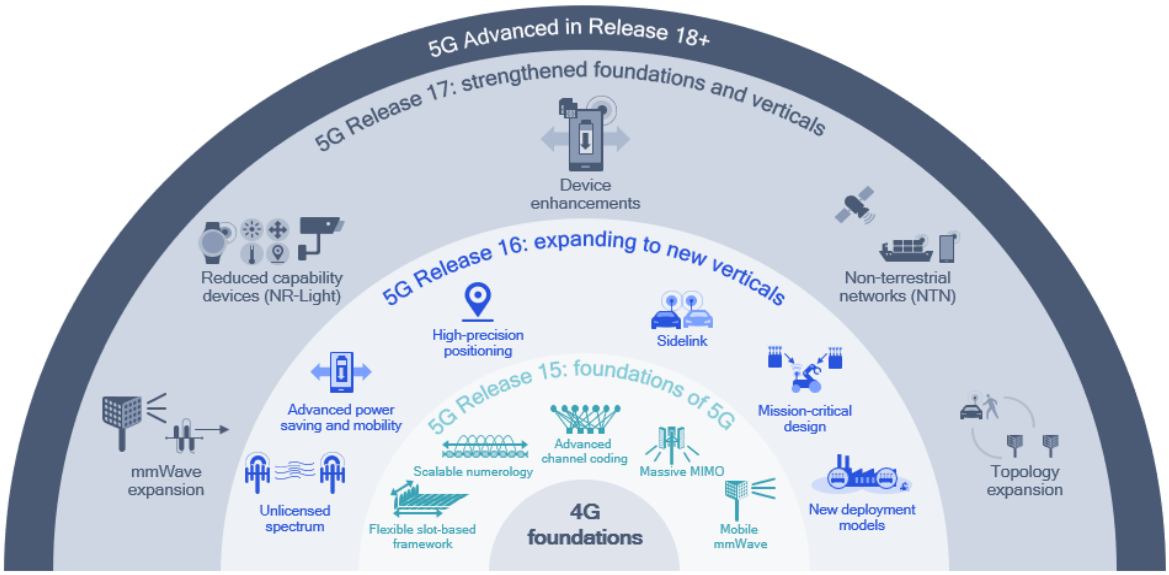

Figure 1.3: Overview of the 3GPP Releases [93].

Doing a brief comparison between the latest NR technology and the existing LTE technology, it is easy to point out some remarkable improvements:

- Use of additional higher frequency bands, particularly mmWave frequencies, greatly expanding the range of spectra and thus enabling much wider transmission BWs with both high traffic capacity and extreme data rates in implementations of small cell-based networks characterized by reduced inter-cell interference levels.

- An ultra-lean design, effective to diminish the volume of transmissions done by the network nodes regardless the amount of user traffic. These ‘always on’ signals, can carry out considerable negative effects in ultra-dense networks whether by imposing network energy performance limits or by causing cell-interference, ultimately leading to a reduction of achievable data rates. In NR, for example, the highly used reference signals for channel-estimation are only present when there is data being transmitted.

- The forward compatibility, with the goal of creating an existent radio-interface design not only capable of responding to the actual user needs but also able to assure good incorporation of future technology release improvements, use-cases, and requirements.

- Low latency support, a requirement that has impacted the design details of many NR layers such as Radio Link Control (RLC) and Medium Access Control (MAC), for example, with the creation of new header structures capable of processing information without previous knowledge of the exact amount of data to transmit.

- A Beam-centric design and multi-antenna transmission, a key feature that provides support for many steerable antenna elements in both transmission and reception, either capable of exploring the advantages of providing extended coverage in higher frequency bands or by enabling massive MIMO (mMIMO) implementations at lower frequencies, allowing the concentration of transmitting antenna power in more narrower beams that can be focused on desired directions with much-less multi-user interference. These higher degrees of freedom (DoF) translate into much improved link reliability and diversity gains and can also be applied for control-plane procedures such as IA. Additionally, a major difference towards LTE is that all the NR channels and signals have been designed to support beamforming (BF), which caused a different reference signal design with each control channel, carrying scheduling decisions in the DL and providing feedback information in the UL, to have its own dedicated reference signal.

1.3 Motivations and Objectives

The mobile networks have become one of the most successful worldwide communication methods, with each succeeding generation being driven by a need to improve and provide more advanced features to address the challenges not overcome by its predecessors. Due to the fast growing pace of high-speed mobile broadband demands triggered by the exponential increase of the number of users and distinct sets of requirements associated with the new wide range of possibilities and specific services to be enabled by the future mobile communications, the IMT-2020 set of specifications, mostly known as 5G, which are being developed by 3GPP according to a published set of recommendations that represent the basis for the implementation of 5G Radio Access Networks all around the world [26]. To fulfill the 5G performance requirements for different use cases, the usage of mmWave spectrum has been considered as a key technology to enable large radio BWs, overcoming the currently saturated frequency spectrum below 6GHz, used in LTE mobile systems.

However, the use of higher frequencies for wireless communications are restricted by the harsher propagation characteristics of the mmWave systems, that become even more hostile as the frequency increases [27].

To efficiently surpass these impairments, NR communication systems benefit from the shorter wavelengths to enable more sophisticated processing techniques such as BF, capable of providing highly precise directional transmission links over multiple receive and transmit antenna elements, each one with detailed control of both phase adjustment and amplitude scaling to provide both high Antenna Array (AA) and spatial multiplexing gains, overcoming the severe high path losses of the mmWave systems [28]. Nonetheless, to achieve the most possible connectivity, there is a need to ensure that the established beamformed connection with each device occurs in the best possible set of beams.

This led to the creation of a distinct set of interoperable procedures known as Beam Management (BM) procedures, mainly consisting on a variety of control tasks, such as the determination of a suitable beamformed beam-pair for idle users, establishing a connection between the device and the network, the retention of the best connectivity possible for already connected users through beam tracking processes, or even the beam recovery procedures needed to reestablish the connection with minimal delay after blockage events, gradual changes in the environment radio propagation conditions or additional user movements and rotations [29], [30].

The Initial Beam Establishment (IBE) stage is the first of the three defined 3GPP BM procedures that aims at establishing the best beam pair in the DL and UL directions. This is usually done by measuring the different Reference Signal Received Power (RSRP) values for each of transmit-receive candidate beam pairs in a dual-end beam sweeping procedure, defined as procedure P-1 [29]. The correspondent beam pair link with the highest RSRP value will be chosen as it ideally experiences the best channel conditions available. Therefore, relevant metrics to perform beam-pair comparisons are fundamental in NR mobile systems for establishing the most suitable available connection.

The work presently done within the framework of this dissertation falls in this context. The main goal consists in a deeper comprehension of the 5G NR BM procedures and requirements defined in the 3GPP standards for the IBE stage. Furthermore, the design and subsequent performance evaluation in terms of Bit Error Rate (BER) of a new 3GPP-standard compliant beam pair selection algorithm based on the SSSs angle estimation (BSAE) is also performed. This BSAE algorithm is implemented in a NR system model that uses BM techniques at both transmitter (TX) and RX ends to establish the beamformed connection in the DL direction by choosing the best Beam-pair available for further synchronization, demodulation and decoding of a live gNB signal.

1.4 Contributions

The main contribution of this dissertation include:

- The design of a new 3GPP-standard compliant algorithm that aims to improve the beam-pair selection stage by using multiple Synchronization Signal Blocks (SSBs) to maximize the RSRP value at the receiver, considering the equivalent channel propagation matrix estimation based on SSSs, to subsequently enhance the overall system performance.

- The simulation and performance analysis comparison of different beam-pair selection algorithms employed in a NR system that makes use of BM procedures at both TX and RX ends for the IBE process.

1.5 Structure

This dissertation is organized into five chapters and starts with an introductory overview of the mobile communication systems evolution along with their main respective correspondent adopted technologies towards the 5G appearance. Afterwards, the motivations and objectives are also presented. The remainder of this dissertation is organized as follows:

- **Chapter 2: 5G New Radio Overview** – This chapter starts with a brief description of some key enabler technologies and techniques used in 5G NR namely, the Orthogonal Frequency Division Multiplexing (OFDM) modulation scheme used in this work, the description of spatial diversity, spatial multiplexing and BF concepts brought by MIMO systems, and the usage of mmWave spectrum alongside its conjugation with mMIMO systems. Next, an overview of some 5G NR details needed to provide a better understanding of the following BM procedures, in particular the new frequency bands used, the transmission structure, the Bandwidth Parts (BWPs), and an outline of the Radio Interface architecture is presented. Finally, the DL Physical Layer (PHY) channels and signals are also described and contextualized.

- **Chapter 3: Beam Management Procedures** - This chapter provides a more detailed description of the essential BM procedures involved in the IBE stage that aim at establishing a suitable beam pair for further communication between the TX and the RX. These procedures include beam sweeping techniques for SSB transmission and reception as well as beam measurement and determination techniques used to determine the best beam pair link with the maximum RSRP value. Moreover, cell search and selection procedures are also presented to provide initial System Information (SI) to the User Equipment (UE) so it can effectively communicate with the network.

- **Chapter 4: Simulation of the Proposed Beam Pair Selection Algorithm –** In this chapter, an efficient proposed beam pair selection algorithm for the IBE stage is presented in detail. We start by analyzing a conventional beam pair selection algorithm through the characterization of the TX and RX models alongside with the channel description, focusing the main BM procedures in IBE. After, the proposed beam pair selection algorithm that uses channel estimation based on SSSs is evaluated in terms of BER against the standard one as well as against an optimal beam pair determination algorithm.

- **Chapter 5: Conclusions and Future Work** - In this chapter, we point out the main conclusions of this work summarizing the main achieved results, and some guidelines for future research and improvements are presented.

Chapter 2

2. 5G NR overview

The exponential growth of the wireless communications systems brought even more demanding requirements for 5G. The fast adoption rate of new users is expected to continue alongside their requests for enhanced applications, digital services, and improved performance. To provide this, 5G NR is based on several different key technologies like OFDM, a highly spectral-efficient modulation technique, the use of mmWave spectrum and mMIMO, that combined makes use of multiple antennas to provide transmissions with increased data throughput, coverage, more network capacity and reduced multi-user interference [31], [17]. The aim of this chapter is to present some of the key enabler technologies and techniques used in 5G NR systems to overcome the limited BW shortage of the LTE systems.

2.1 OFDM Modulation

The OFDM is a multi-carrier modulation concept that consists of a frequency division multiplexing (FDM) scheme where the data signal is divided into different encoded sub-streams which are transmitted by multiple closely spaced orthogonal sub-carriers. Thus, each sub-stream has both a lower symbol rate and reduced BW occupation while each sub-carrier is modulated with a conventional modulation scheme such as Binary Phase-Shift Keying (BPSK), Quadrature Phase-Shift Keying (QPSK) or M-ary Quadrature Amplitude Modulation (M-QAM) [32].

These narrowband OFDM sub-carriers overlap to achieve higher data throughputs while being orthogonal to each other, a feature that heavily reduces the Inter-Symbol-Interference values (ISI) and provides improved spectrum and BW efficiency without a complex channel equalization at the RX, an operation usually done in single carrier systems [33].

In Figure 2.1, the orthogonality concept is illustrated by the data transmission along multiple simultaneous sub-carriers with their correspondent peak values aligned with the null points of other overlapped subcarriers, therefore reducing the Inter-carrier Interference (ICI) while providing a good spectral efficiency, useful to an effective signal recovery.

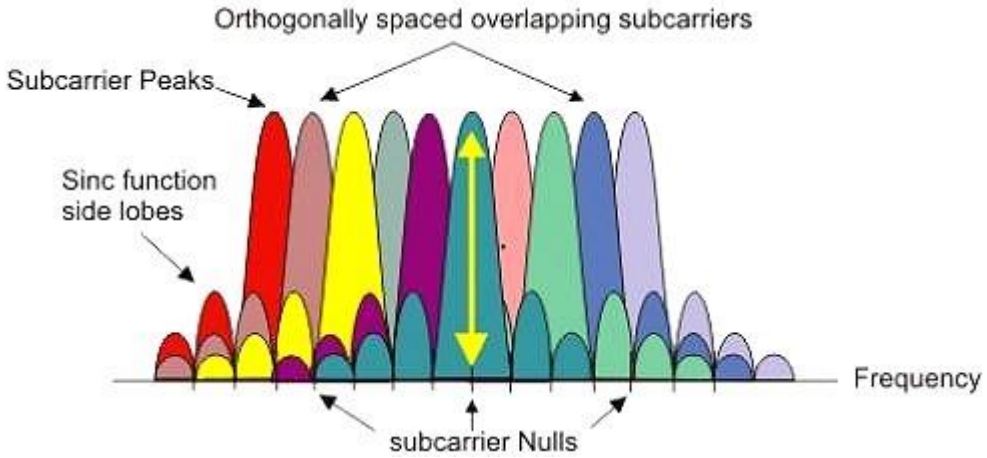

Figure 2.1: OFDM signal frequency spectrum [34].

This OFDM orthogonality is also responsible for additional resilience against frequency-selective fading, multi-path fading and co-channel interference [35]. Additionally, another important concept is the insertion of a defined duration cycle prefix (CP), attached at the start of each OFDM symbol within the subframe, repeating the end of another OFDM symbol. This CP is used to accommodate the delay spread of the channel while effectively avoiding the distortion caused by the ISI for duration values higher than the maximum delay spread of the multipath channel [36]. Furthermore, it is also important to mention the increase of the symbol duration value along with the increase of CP values, consequently leading to a decrease in the transmission rate. Lastly, to an effectively ICI avoidance, the Subcarrier Spacing (SCS) must be much higher than the maximum Doppler shift [37]. These features allow more efficient system implementations with simplified TX and RX designs using Inverse Fast Fourier transform (IFFT) and Fast Fourier Transform (FFT) algorithms, at the TX and RX sides, correspondingly [33], [38].

A conventional OFDM system is presented in Figure 2.2. First, the modulation process starts in the TX with the digital modulation of a bit stream into data symbols to be posterior mapped into the OFDM frame. Later, these symbols suffer an IFFT that is responsible for the signal frequency domain conversion into the time domain. Lastly, the CP is added to preserve the OFDM orthogonality. The signal is then transmitted through a wireless channel where the transmitting information may be affected by different channel conditions such as fading. At the RX side, the CP is then removed and the signal passes through a FFT that converts the time domain signal into the frequency domain, where the equalizer is applied (based on channel estimation) to remove the channel effects. Finally, the information is then de-mapped followed by the demodulation process for the data bits effective recovering.

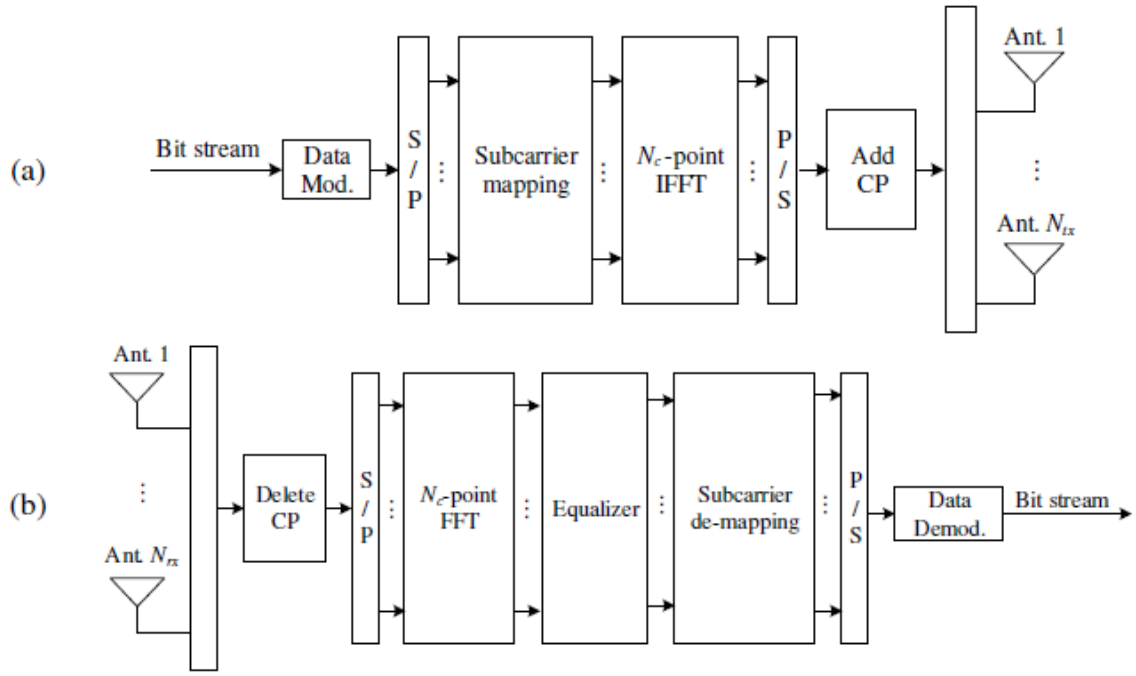

Figure 2.2: OFDM block diagram: (a) transmitter; (b) receiver.

2.2 Conventional MIMO Systems

MIMO is the term used to describe the application of multiple transmit and receive antenna elements both at the TX and RX with the aim of achieving simultaneous transmission of multiple signals, enhancing the transmission data rates, directivity, the channel robustness, and the system spectral efficiency [39]. This antennas scheme provides more DoF than previous configurations but also presents some drawbacks at both hardware and software levels. In terms of hardware, the increasing complexity of the full digital architectures, where there is one dedicated Radio Frequency (RF) unit connected to each antenna, results in higher cost and power consumption. In terms of software, the need of additional computationally intensive signal processing algorithms and their additional power consumption presents some challenges for the systems optimization [40]. Additionally, with the use of a higher number of antennas, more RF interference occurs, and the antennas correlation values become even more important.

To improve the overall system performance taking advantage of the usage of terminals with multiple antennas, the use of MIMO technology, presents different benefits without an additional increase in BW or transmit power, presented in Figure 2.3 [41]:

- Spatial Multiplexing gain, increasing throughput rate and system's capacity with the transmission of information in multiple parallel independent data streams that share the same set of time and frequency-domain resources.

- Spatial Diversity gain, improving the link reliability and robustness to co-channel interference by placing the antennas appropriately apart to create independent

transmission paths with low uncorrelated fading values between them. The transmission probability error can then be decreased by averaging over these multiple independent signal paths and hence, obtaining the desired diversity gain.

- Array gain, by using the multiple transmit antennas to perform BF, directing the transmitted signals to the UE with improved Signal-to-Noise Ratio (SNR).

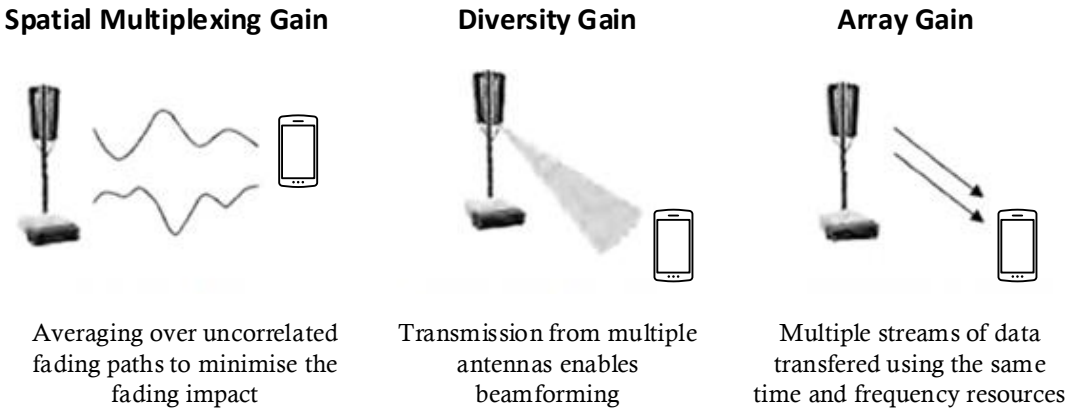

Figure 2.3: Benefits of MIMO systems [42].

For those reasons explained above, MIMO has come to be the adopted technology in LTE systems with its first specification standards defined in 3GPP Release 8, back in 2008, enabling the use of the first 2 TX/2 RX variation, called 2x2 MIMO. This initial version experienced numerous critical enhancements over the subsequent releases, especially concerning processing power rates, ending up enabling the usage up to 8 DL transmission layers and spatial multiplexing up to 4 UL layers in the current LTE Advanced 4G networks, specified in Release 10.

2.3 Millimeter-Waves and massive MIMO

The combination of mmWave and mMIMO complement each other and represent two important 5G enabling key technologies used to overcome the limited BW constraint, high data rate and spectral efficiency requirements of the modern mobile systems.

Frequency bands from 30 to 300 GHz in the electromagnetic spectrum are also known as mmWaves due to their associated wavelengths between 1mm and 10mm. This Extremely High Frequency (EHF) spectrum [43] is mostly unexploited and thus, presents a particularly important resource for the future of the mobile communication systems since it can offer wide channel BW and escalating capacity demands useful for a wide range of new possibilities, use-cases and 5G scenarios [44].

MmWave mobile communication systems capable of achieving gigabit-per-second data rates in urban deployments have been already studied [45], [46]. Still, the use of this mmWave frequencies is constrained to much different propagation characteristics than the most utilized nowadays sub-6GHz microwave frequency bands, with favorable propagation conditions. Different difficulties,

such as increased free space pathloss, shadowing effects and many attenuation loses that become even more relevant at more higher frequencies cannot be neglected.

On the other hand, a particular case of the MIMO systems is the mMIMO that uses hundreds of antennas to allow the transmission and reception of a signal through beams with narrower BW and higher gain value. Moreover, there is also the possibility to adjust both amplitude and/or phase values of each RF chain, thus, providing an active control of the beam direction, concentrating the transmit power towards the UE location. This feature allows to reduce the problem caused by high attenuations in mmWave, hence it is considered a promising combination. In mMIMO, the larger number of additional steerable antenna elements are also used to dynamically assign beams in a specific direction allowing the transmission of multiple data streams while at the same time, providing much greater adaptivity, user throughput, network capacity and improved UE signals with reduced interference without an additional increase in BW or transmit power [28].

2.4 Analog, fully digital and hybrid architectures

The adaptative BF can be applied at either BS or UE ends with the goal of establishing the Beam-pair that leads to the best connectivity possible. By adjusting the phase values between the transmitted/received signals, it is possible for both the TX and RX to have a more precise control of the angle at which the constructive frequency occurs, maximizing the beam gain towards the desired UEs while minimizing the leakage power of intrusive signals originated from unwanted spatial locations. This mechanism can be applied via analog, digital or even a combination of these two domains, also known as hybrid architectures, as shown in Figure 2.4.

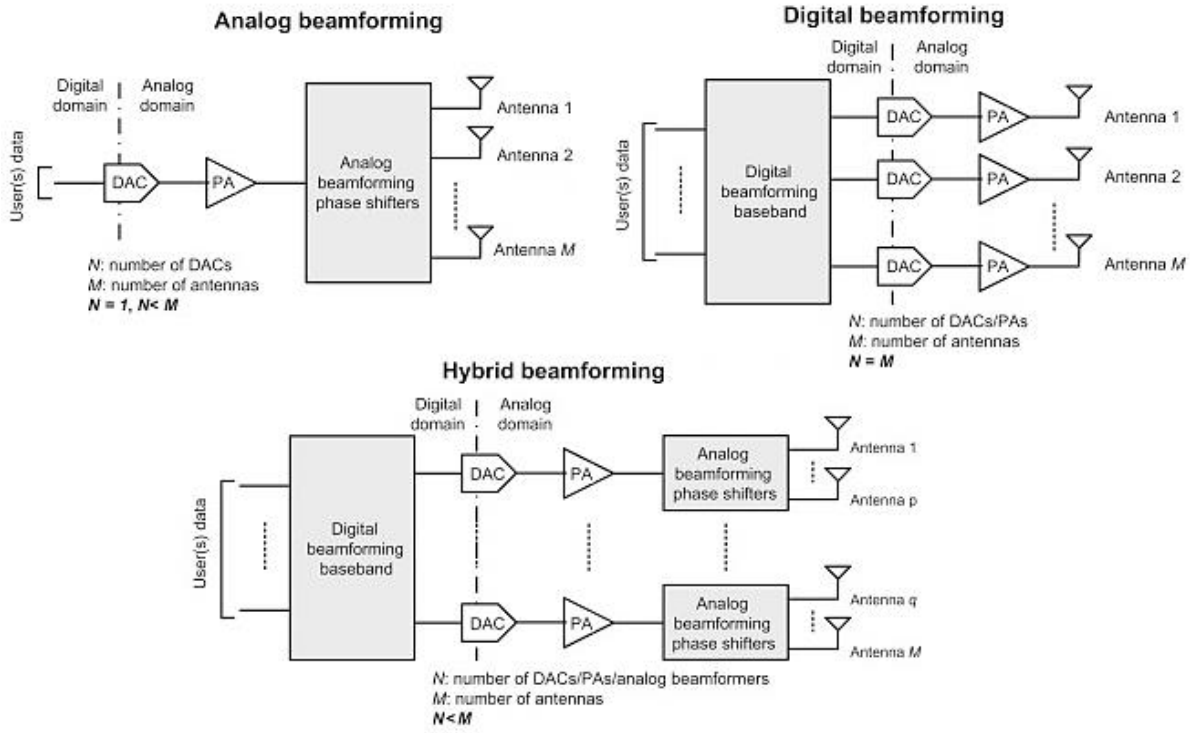

Figure 2.4: Beamforming architectures [47].

In fully analog BF architectures, Power Amplifiers (PA) and digitally phase shifters (PS) are implemented to reduce both the system's complexity and power consumption [48], where an analog signal which has been previously processed in the digital domain is then divided into separate paths. The application of the set of BF weights to the RF signal generate a single beam that can be directed towards one or multiple UEs being served in the same direction at that point in time. This method has the advantage of requiring only one Radiofrequency (RF) chain for all antenna elements however, in practice, analog BF techniques do not explore all mMIMO resources because the formed beams are either fixed or steered at a much slower rate compared to digital BF, consequently imposing limits to the achievable system performance and effective capacity.

On the other hand, fully digital architectures require one dedicated RF chain per antenna element and thus, since mMIMO implementations comprehend a very large number of antenna elements, their implementation is not practical due to the increased power consumption, complexity and higher hardware component costs needed for mmWave frequencies applications, like power amplifiers (PA) and digital-to-analog converters (DACs) using alternative semiconductor technologies. To maximize the diversity and multiplexing gain in the MIMO environment, unlike the fully analog BF technique, the digital BF technique performs BF in the digital domain using the baseband signal operation where digital amplitude and phase weighting is performed in multiple parallel RF chains, allowing the simultaneous generation of multiple beams that can be separated and directed towards the UEs.

To overcome the performance limitations of analog architectures and the cost/power consumption limitations of digital architectures, hybrid architectures have been proposed, where some signal processing is done at the digital level, and some left to the analog domain. This structure allows combining the advantages of both analog and digital BF techniques while reducing hardware complexity in a mMIMO environment are seen as a promising solution [46]. In this method, a more energy-efficient implementation is presented where each data stream has a separate analog beamforming unit (BFU) with a set of antennas, reducing the total number of RF chains in the system while preventing performance losses.

2.5 Overall Radio Interface-Architecture

The 5G systems (5GSs) are composed by the 5G Core Network (5GC), the Radio Access Network (RAN) and the UE, as presented in Figure 2.5.

The 5GC is a service-based architecture responsible for non-related radio access functions needed to provide a complete network, thus, providing connectivity both to internet and application servers while offering flexibility in terms of functionality. This is specially observed in the split of user-plane and control-plane functions, allowing independent scalability, evolution, and different deployment strategies.

The 5G NG-RAN, by its turn, is responsible for all the radio-related functions of the overall network such as scheduling processes as well as the multi-antenna schemes [2]. For assuring backwards compatibility, the new RAN supports two types of logical nodes defined in 3GPP: the gNB and the next generation eNB (ng-eNB) for LTE devices [49]. These nodes are responsible for

all the radio-related functions in one or more cells, including radio resource management and connection establishment, among others [50].

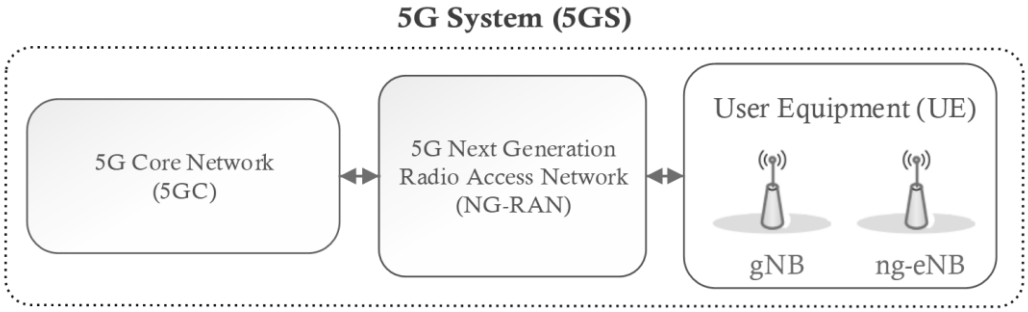

Figure 2.5: 5G System (5GS) illustration.

A more detailed overview and overall description of the NG-RAN architecture with its various interfaces and their interactions is presented in 3GPP TS 38.300 [49] and 3GPP TR 38.801 [50]. Additionally, a more complete description of the 5GS CN architecture model and concepts, including the user plane and control plane split can be found in 3GPP TS 23.501 [51] and 3GPP TS 38.401 [52].

One important characteristic of the NG-RAN is the split between user plane and control plane functions allowing independent scalability, where the user plane protocol stack is responsible for carrying information between the end user and the application server while the control plane stack is responsible for transmitting signaling messages further used for connection setup, mobility and security [42].

The Radio Resource Control (RRC) is the only control plane protocol stack that is not present in the user plane context. It is used for signaling between the UE and the BS, handling RAN-related control-plane procedures like the broadcasting of System Information (SI), needed for the UE to be able to communicate with a cell, or the connection management, configuring all the necessary parameters for communication between the UE and the RAN. This RRC layer is particularly relevant in the BM procedures and will be later discussed in chapter 3.

A general overview of all the different user/control plane protocol entities in the NG-RAN between the UE and the gNB is presented in Figure 2.6, as well as a brief description of each of their layer's functions in Table 2.1.

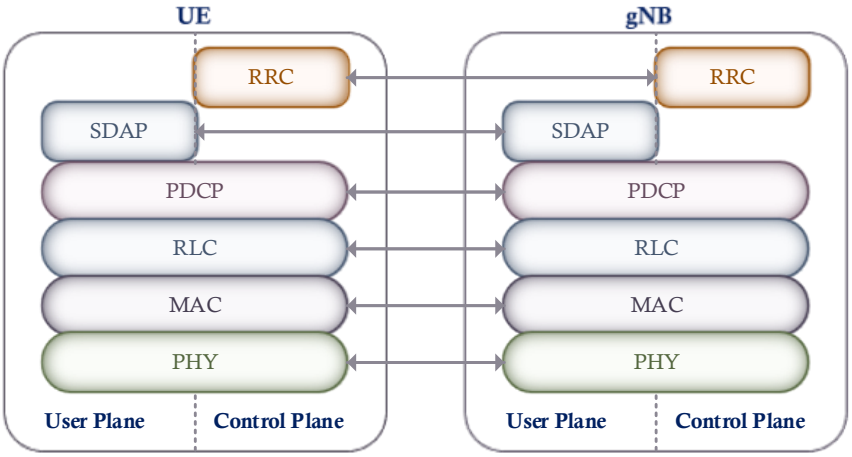

Figure 2.6: User Plane and Control Plane protocol stack.

Table 2.1: Main functions of the different protocol entities.

Layer	Functionalities
Radio Resource Control (RRC)	• Signaling messages (3GPP TS 38.331)
Service Data Application Protocol (SDAP)	• Mapping QoS Flows of 5G CN data to radio bearers based on their requirements (3GPP TS 37.324)
Packet Data Convergence Protocol (PDCP)	• header compression • Integrity protection • Ciphering • In-sequence delivery retransmissions to highest layers • Routing and duplication (3GPP TS 38.323)
Radio Link Control (RLC)	• Segmentation and retransmission handling (3GPP TS 38.322)
Medium Access Control (MAC)	• Multiplexing of logical channel data from RLC • Hybrid-ARQ retransmissions • Scheduling related functions • Provides services to RLC in form of logical channels • Generates Transport blocks from the original channel data to pass to PHY (3GPP TS 38.321)
Physical Layer (PHY)	• Coding/Decoding • Modulation/Demodulation • Multi Antenna Processing

	• Mapping the signals to appropriate physical time-frequency resources (3GPP 38.211; 38.212; 38.213; 38.214)

More detailed information about the user plane protocol can be found in 3GPP TS 38.425 [53]. In addition, the user plane and control plane are also described in 3GPP TS 38.300 section 4.4 [49]. Finally, a better description of the RRC protocol can also be found in 3GPP TS.300 section 7 [49] and in 3GPP 38.331 [54].

For the sake of simplicity, in this dissertation there is only the focus on the Physical layer (PHY), also known as Layer 1 (L1).

2.6 Transmission Structure

The following subchapters aim to deliver a better insight of the flexible resource allocation in the 5G technology, crucial to provide an efficient support for numerous devices with different transmission capabilities.

2.6.1 Time-Domain Frame Structure

The NR time-domain structure is composed by an indexed 10ms duration radio frame using the System Frame Number (SFN) and is equally divided in 10 subframes of 1ms each one. Each subframe is, on the other hand, composed by slots consisting of a fixed number of OFDM symbols as shown in Figure 2.7. As the numerology increases, the number of slots per subframe also increases, causing the reduction of each slot duration and therefore resulting in the increase of the number of symbols sent in a determined time. Using Normal CP values, the slot is composed by 14 OFDM symbols whether in Extended CP mode there is only 12 OFDM symbols per slot [55].

Since the slot is defined by a fixed number of OFDM symbols (N_{symb}^{slot}), there is a possibility to reduce the slot duration by using numerologies with higher SCS values, however, the CP duration is also decreased. Thus, this methodology cannot always be feasible to support low-latency communications because of the drawbacks in scenarios where there is a long delay spread that might results in not enough provided CP protection against inter-symbol Interference (ISI).

A more efficient approach to achieve low latency communications is done by enabling transmissions over a fraction of a slot subsequently minimizing the decoding delay, a feature sometimes referred as “mini-slot” transmission [56]. These types of transmissions enable the immediate transmission of mini-slots containing a reduced number of OFDM symbols (2, 4 or 7 symbols), being capable of providing a quick delivery of low-latency data needed in URLLC scenarios [57]. This is also particularly useful in NR unlicensed (NR-U) spectra operation, introduced for the first time in the 3GPP release 16 supporting the existing global 5GHz and 6GHz unlicensed bands widely used by Wi-Fi and LTE technologies nowadays, and the later expansion to the unlicensed 60 GHz band (57 to 71 GHz) available for 5G deployment, for both public and private networks [24]. In NR-U operation, the TX commonly applies the “listen-before-talk” procedure to certify that the radio channel is not already occupied with other transmissions and, as soon as the

channel is declared available, it is advantageous to immediately start a transmission rather than wait until the start of the slot, greatly avoiding channel occupation from other devices and hence, improving the system efficiency.

Besides the better support for very low latency communications and unlicensed spectra, there are several benefits in occupying only a part of the slot for transmission, for example, with the use of analog BF, where it can only be used one beam at a time in transmissions to multiple devices using different beams, resulting in the need for time-domain multiplexing of the different devices. In this situations, with the large BW available in the mmWave spectrum, a few OFDM symbols can be sufficient to carry the available payload.

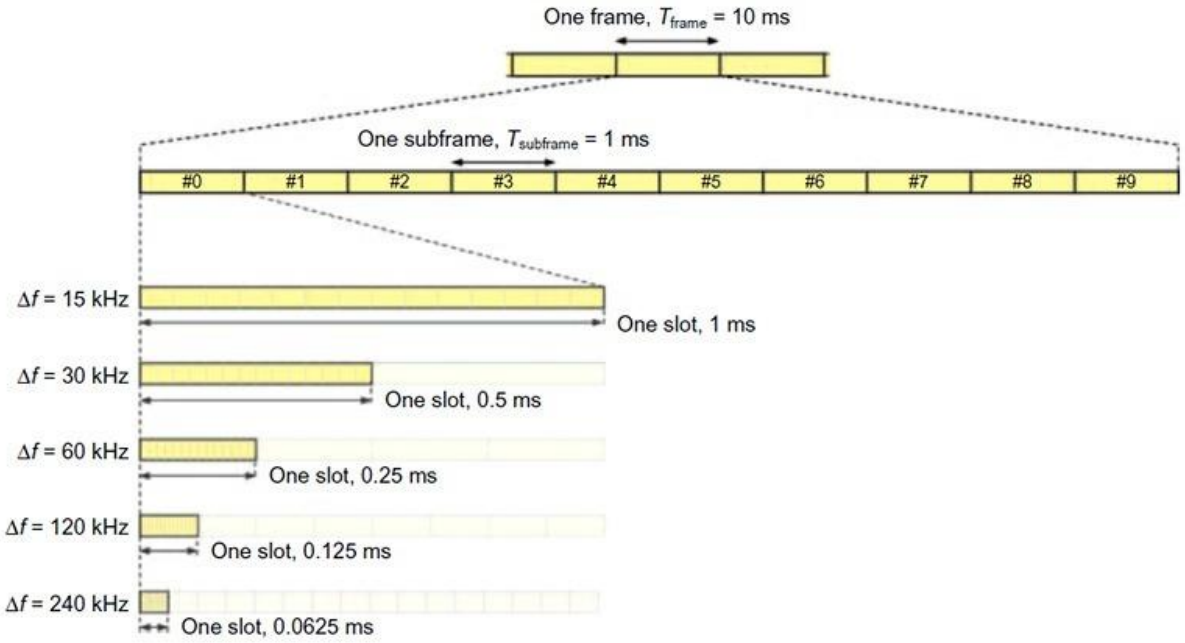

Figure 2.7: Subframe and slots in NR (Normal CP values assumed) [2].

2.6.2 Frequency-Domain Frame Structure

In similarity to LTE, NR technology is based on OFDM modulation due to its robustness to time dispersion and ease of exploiting both the time and frequency domain resources while defining the structure for different channels and signals [58].

In the already mentioned 3GPP Release 17, specification of multiple OFDM numerologies to provide flexible resource allocation for a wide variety of deployment scenarios and electronic devices transmission's capabilities is presented [49]. To withstand implementations from using large cells, operating at lower frequencies, to mmWaves systems with very wide spectrum allocations, NR supports a flexible OFDM numerology (μ) with SCSs from 15 to 960 kHz and its correspondent proportional change in the Cyclic Prefix (CP) duration for a DL or UL BWP [55]. This SCS value is responsible for frequency domain BW determination and the time domain duration of a single Resource Element (RE), the smallest physical resource in NR, with the respective dimensions of 1 subcarrier in the frequency domain and 1 symbol in the time domain. Furthermore, a set of 12

consecutive subcarriers in the frequency domain is defined as a Resource block (RB), as illustrated in the Figure 2.8:

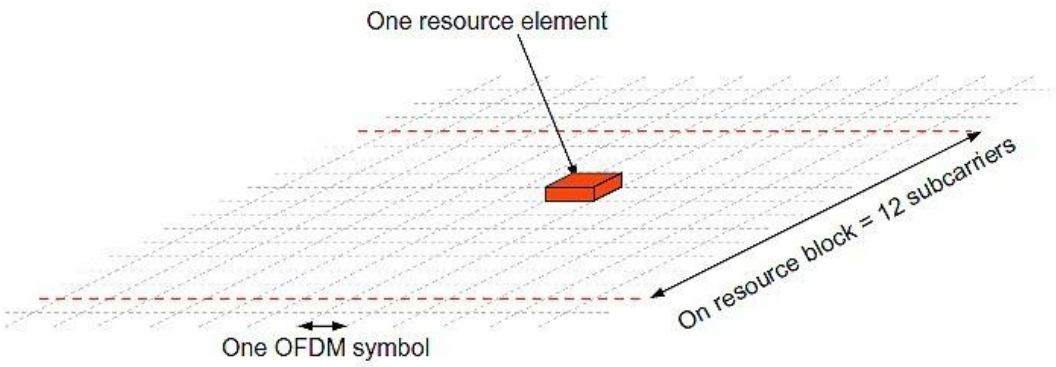

Figure 2.8: Resource Block and Resource Element illustration [2].

The NR numerology configurations are presented in Table 2.2, where μ=0 corresponds to the previous LTE technology subframe configuration with the SCS value fixed at 15 kHz, which is beneficial to coexistence purposes while the new possibility of scaling SCS values up to 960 kHz can assure the stricter latency and QoS demands of a wider range of services [59]. The use of a smaller SCS value can provide a long CP value while higher SCS values are useful, for example, to deal with the increased phase noise at higher frequencies.

Table 2.2: Supported transmission numerologies [55].

μ	$\Delta f = 15 \times 2^{\mu}$ [kHz]	CP	Nº slots/ frame ($N_{slot}^{frame,\mu}$)	Nº slots/ subframe	Slot duration (TTI)	Resource Block Bandwidth	
0	15	Normal	10	1	1ms	180 kHz	FR1 use
1	30	Normal	20	2	500μs	360 kHz	
2	60	Normal, Extended	40	4	250 μs	720 kHz	
3	120	Normal	80	8	125 μs	1.44 MHz	FR2 use
4	240	Normal	160	16	62.5 μs	2.88 MHz	
5	480	Normal	320	32	31.25 μs	5.76 MHz	
6	960	Normal	640	64	15.625 μs	11.52 MHz	

Another major difference towards LTE is related to the maximum carrier BW value in NR as stated in the last subchapter. Even though the same total of up to 3300 subcarriers can be used, the maximum carrier BW can take values up to 100MHz for FR1 or 2000MHz for FR2. Additionally, there is also the possibility of combining different numerologies within the duration of a single symbol [60], [61]. A more detailed presentation of which numerologies can be used within each operative band is presented in 3GPP TS 38.104 [62].

2.7 Bandwidth Parts

Another new concept in NR is a feature known as BWPs, a subset of contiguous Common Resource Blocks (CRBs), a set of RBs which occupies the channel BW and aims to provide more flexibility by enabling the multiplexing of different numerologies with different signals and signal types to be transmitted in the same carrier for better efficient use of spectrum and power resources [55]. Due to the wider possible range of BWs in NR and the different UEs capabilities, the challenge of using the larger available BWs can be surpassed using BWPs, sub dividing the carrier and using it for different purposes. In this way, if a device can process the simultaneous reception of multiple BWPs, the mixing of different numerologies in a carrier is possible. Despite this new possibility, some interference problems with subcarriers of another technology, known as Inter Numerology Interference (INI) may arise, introducing new challenges in the way waveforms are built and managed [57], [61].

The Figure 2.9 illustrates some of the new possibilities associated with the flexible use of BWP, where the BS and the UE different capabilities do not need to match, thus, the BWPs are therefore used to provide services to UEs that do not support the full channel BW. In the first case, the UE is assumed to only support a reduced channel BW and the BWP is used to provide services with a subset of the total channel BW. In the second case, there is the representation of mixed non-contiguous BWPs with different numerologies in a carrier. Finally, the last case represents the insertion of a reduced device energy consumption for each separate user through using a smaller part of the overall subcarrier.

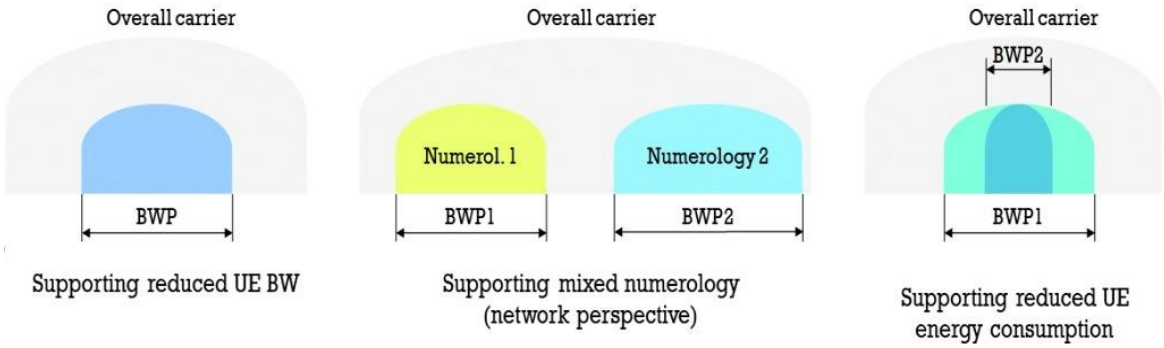

Figure 2.9: Main Bandwidth parts multiplexing possibilities [63].

Regarding configuration purposes, these BWPs can have different configurations, including different numerologies, different frequency locations, BW sizes or even a different Control Resource Set (CORESET). A UE can be configured up to four BWPs per carrier both in the DL and the UL from which only one can be active in each direction, implying that the reception of PDSCH or PDCCH can only be done within an active DL BWP [55]. In a similar way, for the UL, the transmission of the PUSCH or PUCCH can just be done in the active UL BWP. These new specifications create more new test possibilities and permutations in need of validation in 5G NR devices, introducing more complexity to the way 5G NR signals are created and demodulated. A

more detailed description about BWP operation can be found in 3GPP TS 38.213, section 12: "Bandwidth part operation" [64].

2.8 Physical layer Downlink Overview

An overview of the DL PHY layer is presented in Figure 2.10 with its different physical channels and signals. A description of their functions and carried information is also described.

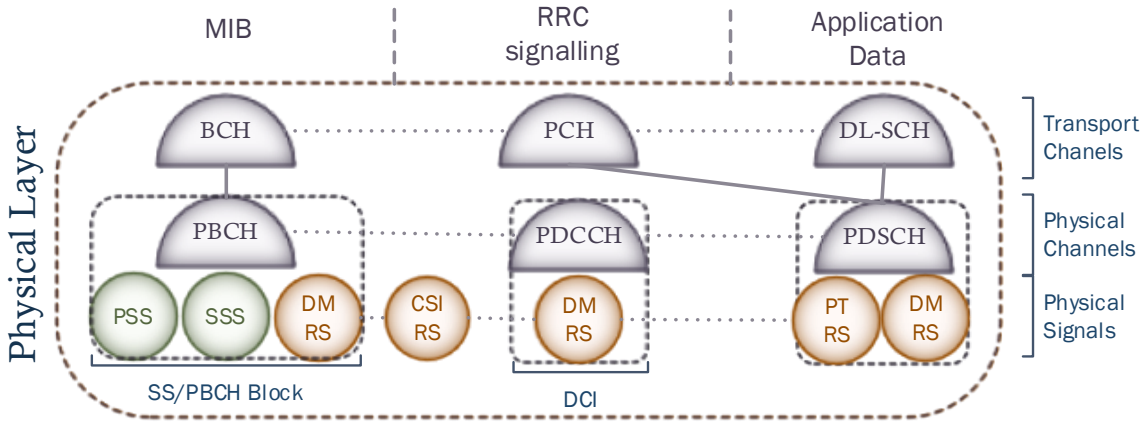

Figure 2.10: Mapping of DL Transport channels onto Physical channels.

2.8.1 Physical Channels

A DL physical channel corresponds to a set of time-frequency REs carrying information originated from higher layers across the air interface. The following downlink physical channels are defined in 3GPP:

- Physical Downlink Shared Channel (PDSCH): is the main physical channel not only used for data transmission but also paging information, Random-Access (RA) response messages, and delivery of SI. This channel is not used to transfer high layer information, so it does not have any associated transport nor logic channels

- Physical Downlink Control Channel (PDCCH): is used for transmission of Downlink Control Information (DCI) in one or more control resource sets (CORESETs), mainly scheduling decisions, required for the correct reception, demodulation and decoding of the PDSCH. For assuring a compatibility between devices with different BWs, the forward compatibility concept and the device-specific BF support on the control channels, a different reference signal design was required with each control channel having its own dedicated reference signal.

- Physical Broadcast Channel (PBCH): is used to broadcast part of the SI, which is needed for the UE to access the network.

2.8.2 Physical Signals

A DL physical signal is used for synchronization, channel state information (CSI) and channel estimation. They are generated and used by the PHY layer without carrying information originated from higher layers. Currently, the following DL physical signals are defined in 3GPP:

- Demodulation Reference signals (DM-RS): used for the PBCH, PDCCH and for PDSCH. They are sequences know to UE that will be further compared with the received signal sequence for channel estimation impact of the propagation channel.

- Phase Tracking reference signals (PT-RS): equally used for UL, is employed as an extension to DMRS for phase-noise compensation within the signal transmission duration. This phase noise is predominantly generated in the oscillators at both the TX and RX, becoming more significant for the higher operating frequency bands.

- Positioning Reference Signals (PRS): is the main reference signal supporting DL based positioning methods, used to provide better levels of accuracy, coverage and interference avoidance or suppression of neighboring cells which can be difficult to measure in scenarios where they are co-channel with the reference cell.

- Channel-state information reference signals (CSI-RS): are a multi-purpose signals intended to be used by the UE to acquire DL channel-state information (CSI) and then perform Channel Quality indicator (CQI) reports. They can also be configured by the BS for time/frequency tracking in BM procedures and for mobility measurements.

- Primary Synchronization Signal (PSS) and Secondary Synchronization signal (SSS): used by the UE during the IA procedure, Physical Cell Identity (PCI) identification, and during other BM procedures. They can also be used for Reference Signal Received Power (RSRP), Signal-to-Interference plus Noise Ratio (SINR) and Reference Signal Received Quality (RSRQ) measurements.

A more detailed description of the physical channels and signals in the DL are presented in 3GPP 38.211, sections 7.3 and 7.4 [55], respectively. Additionally, some more information regarding the physical DL channels is also presented in 3GPP 38.300 in sections 5.2.2 and 5.2.3 [49].

Chapter 3

3. Beam Management techniques in the Initial Beam Establishment context

As mentioned before in the chapter 2, the use of mmWave frequencies is crucial to provide the coverage area extension by enabling AASs with beam-centric design and additional BF gain. Hence, it is of great importance an efficient management of the established beam-pairs used for both transmission and reception of information between the gNB and the UE. To support this, 3GPP specified a set of Layer 1 (L1) and Layer 2 (L2) BM procedures in 3GPP TS 38.802 with the main goal of establish and retain a suitable beam-pair capable of providing the best connectivity possible for transmission, both in UL and DL directions [29].

Since the optimal beam-pair may not always be in a Line of Sight (LoS) scenario between the gNB and the UE, especially at mmWave frequency bands, where there are higher levels of reflection upon static or moving obstacles in the Radio Link Path, a reflected beam-pair can provide a better connectivity, as shown in Figure 3.1. Thus, the BM procedure are also required to handle this situations and support mobility between beams for seamless data transmissions.

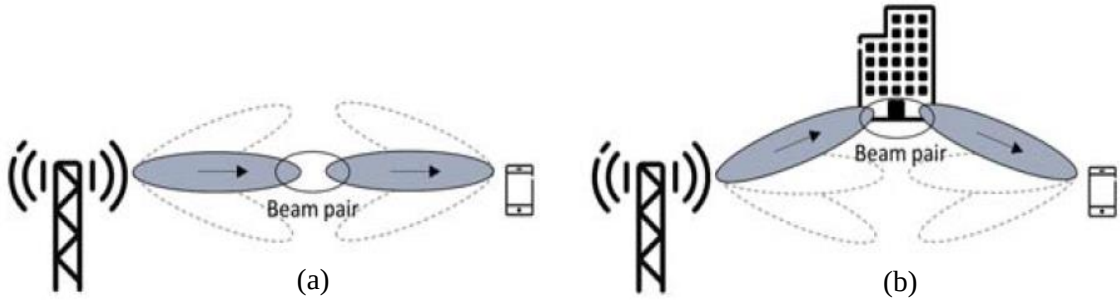

Figure 3.1: Downlink direction Beam-pair establishment: (a) Direct; (b) Reflected [2].

Another important aspect of the beam-pair selection is the possible existence of Beam Correspondence, specified in 3GPP TS 38.101-2 section 6.6 [65]. This concept aims at increasing the efficiency of the BM procedures by making use of the optimal beam-pair selected measurements in DL transmission to select a suitable beam for UL communications, sparing time in the process of selecting another pair for communication in the opposite transmission direction. Otherwise, in case it turns out to be inconceivable to use the same Beam-pair, the UE can still perform UL beam sweeping allowing the BS to complete the beam-pair reselection based upon Sounding Reference Signals (SRS) transmissions.

Usually, BM consist of the following three procedures:

- Beam Establishment: where initial cell synchronization occurs enabling UE measurements on the different TX beams with the purpose of establishing an initial DL beam-pair selection between the gNB and the UE.

- Beam Adjustment: a beam refinement procedure not only used to compensate for the UE mobility effects but also for gradual changes in the environment.

- Beam Recovery: a recovery beam-pair procedure in link failure scenarios that ultimately led to the loss of connection between the UE and the gNB.

This dissertation is primarily focused on the initial beam establishment procedure in the DL as well as beam-pair refinement for transmission performance enhancement purposes. A more detailed view of BM procedures in the Initial Beam Establishment stage will be discussed in more detail in the following sections.

3.1 Introduction

The IBE stage includes the procedures and functions by which a beam pair is initially selected for the DL and UL transmission directions, for example, when a UE enter a coverage area of a system or is switched on, accessing the network to request the set-up of the connection with the gNB.

3GPP TS 38.304 defines some expected functions and procedures for the suitable cell selection by the UE for RRC_IDLE and RRC_INACTIVE states, described in RRC subsection, while still leaving some freedom and flexibility for different implementation designs [66]. The main processes in IBE context are presented in the Figure 3.2, consisting of PLMN selection, the IA stage composed by Cell Search, Selection and RA procedures that allow the device to find a cell to camp on and further receive the necessary SI for the connection set up and finally, the RRC connection establishment. More detailed information about the RRC sublayer and its functions inside the control-plane can be correspondingly found in 3GPP 38.300 Sections 7 and 4.4.2.

The following section of this dissertation will describe the IBE processes involved, as well as Radio Resource Control (RRC) functionality, an important mechanism used to handle the RAN-related control-plane procedures needed for the successful exchange of UE information and 5GC connection establishment, such as the broadcast of SI required for the device communication with a cell.

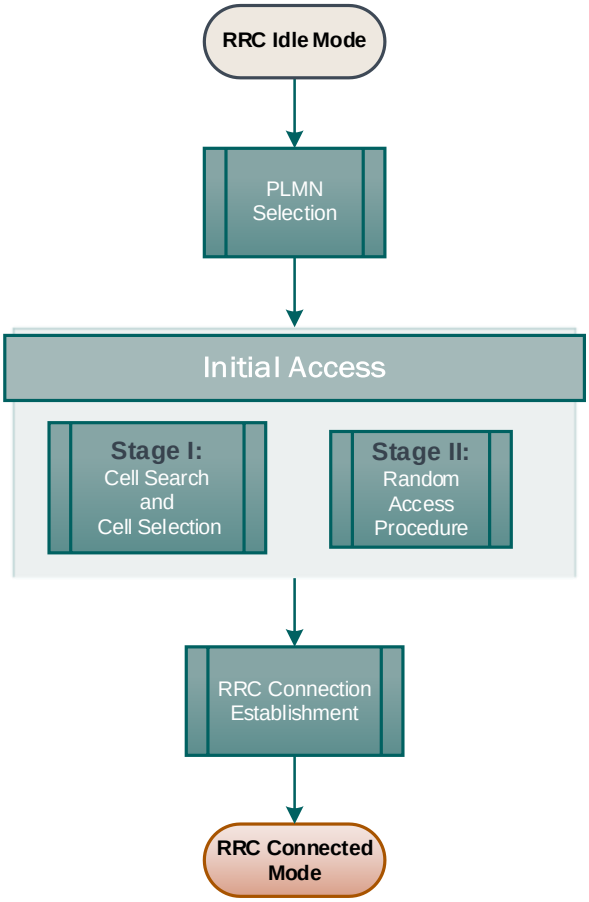

Figure 3.2: Initial Beam Establishment Overview.

3.2 PLMN Selection

The Public Land Mobile Network (PLMN) is defined in 3GPP by a network established and operated for the purpose of providing land telecommunications services to the public, in one or a combination of frequency bands [66]. Its selection can be done either automatically or manually and this process corresponds to the first stage of the Initial Beam Establishment procedure.

The process of PLMN selection can be performed using previously stored information measurements for optimization purposes or, otherwise, with no previous known information, where the process of PLMN selection is accomplished by the UE performing a cell search of the strongest cell on each carrier of every RF channel within its supported frequency bands, as described in the next subchapter. Each PLMN found is identified by its PLMN identity (PLMN ID), acquired from the SI on the broadcast channel within System Information Block 1 (SIB1) and subsequently, based on a RSRP quality metric criterion, reported back to the Non-Access Stratum (NAS) layer, responsible for the PLMN selection [66]. A more detailed description of the PLMN selection process can be found in 3GPP 38.304 Section 5.1.

3.3 Cell Search and Selection

The Cell search stage includes the functions and procedures by which a UE finds cells nearby when entering a system, or new cells to allow efficient mobility while moving within the system, even in RRC_Connected/Inactive states. This is done by the acquisition of time and frequency synchronization with a cell based on the so-called SSBs, specified in 3GPP TS 38.211 as SS/PBCH block, a structure consisting of a PSS, a SSS and a PBCH with associated DMRS, needed for coherent demodulation of the PBCH [55].

This section will start by presenting the SSB structure along with the stage I of the IA, correspondent to the cell search and selection procedure. Additionally, the L1/L2 control signaling associated with the PDCCH transmissions, including the necessary information needed for the UE to receive, demodulate, and decode the PDSCH are also described to provide a better understanding of the process.

3.3.1 SSB and SS Burst set

An SSB is transmitted periodically with a default value of 20ms on a set of time/frequency REs within the basic OFDM grid, consisting of 4 OFDM symbols in the time-domain and 240 contiguous subcarriers (20 RBs x 12 subcarriers) in the frequency domain, as illustrated in Figure 3.3.

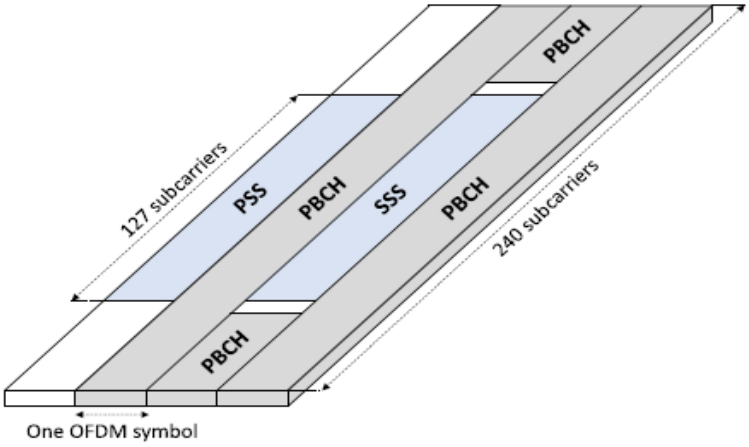

Figure 3.3: Time/frequency structure of a single SSB [2].

This 20ms default value is used as an indication for the UE to know how long it must stay on each frequency before concluding that there are no synchronization signals (SSs) present. Nevertheless, there is the possibility of periodicity configuration for shorter or longer SSB transmissions with values from 5ms to 160ms, useful, for example, to enable a faster cell search in already network connected devices, where beam-sweeping over many beams with a corresponding large number of time multiplexed SS blocks is performed or allowing enhanced network energy performances in mMTC scenarios, respectively [67]. This possibility for faster cell search is even more enhanced in NR by allowing a set of different possible frequency locations for the SSBs within

each frequency band. In this way, instead of fixing the SSs location at the center of the carrier like in LTE, a device without prior knowledge of the frequency-domain carrier position only searches for the SSs in a smaller set of frequency positions that can be used by the UE for SI acquisition, known as synchronization raster [62].

These SSBs can be organized in sets, and it is possible to apply beam-sweeping techniques for their transmission. 3GPP defined an SSB set, or SS burst in TS 38.213 as the set of one or more SSBs within a beam-sweep procedure. These Bursts are used to address the requirements of BF and BM procedures and their periodicity (T_{SS}) is flexibly configurable between the same values described above for the SSB period, however, each SS burst set is always confined to half a radio frame, that is, 5ms time interval, either in the first or second half of a frame. Currently, there are seven different time domain patterns defined by 3GPP from case A to case G, which are used for SSB transmission with different combinations of both SCS and frequency range values [64]. The following Figure 3.4 shows the five first SSB patterns:

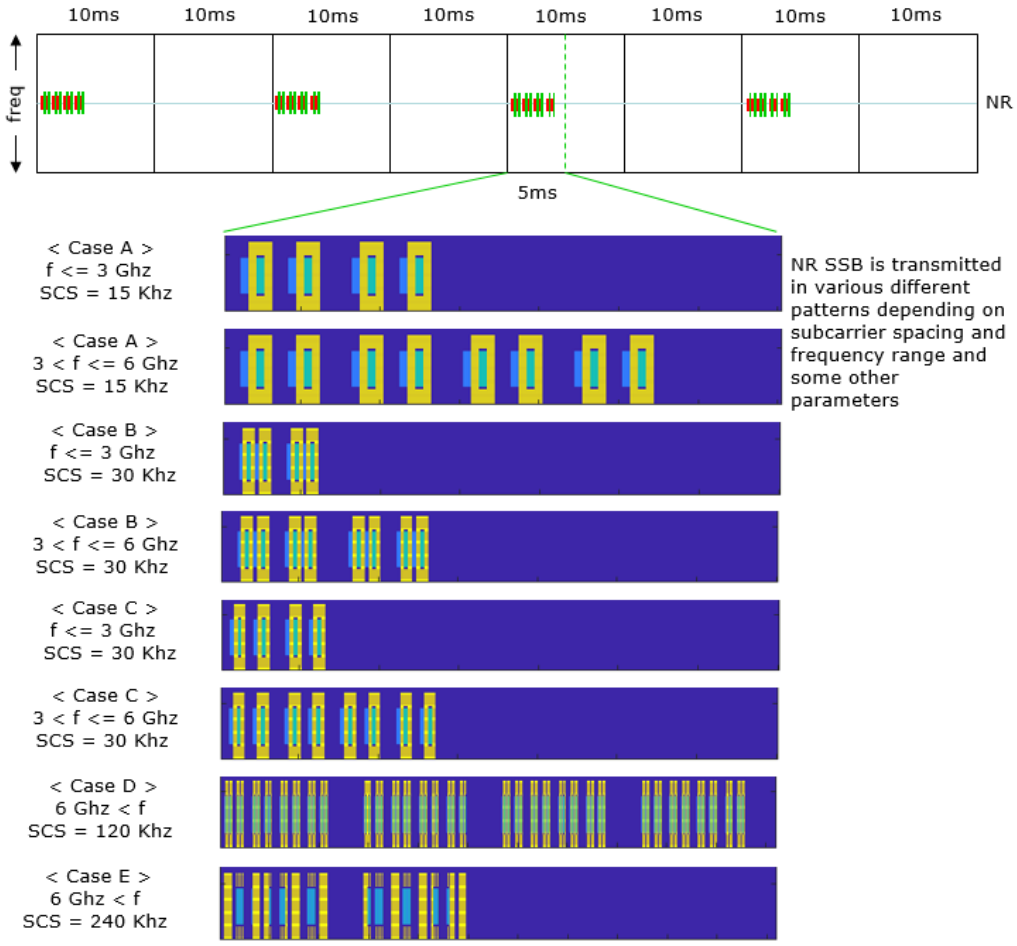

Figure 3.4: Different SSB transmission patterns [68].

Each SSB belonging to an SSB burst is assigned to a different beam as shown in Figure 3.5 and the maximum number of SSBs per burst is also specified depending upon the operating band. For FR1 bands below 3GHz, there can be up to 4 SSBs within a SSB set, while the remaining FR1 bands

can have a maximum of 8 SSBs per SS Burst set. Otherwise, FR2 bands can achieve a higher number of 64 SSBs per SS burst set, enabling beam sweeping techniques over 64 beams, mainly because of the use of more narrow centric beams in this range of frequencies [64]. Even though there is a limitation to the maximum number of used SSBs, the gNB still has the freedom not only to define the number of allowed SSBs within a burst but also how to distribute them in any possible spatial locations. More information regarding the set of SSBs in a burst for each case can be found in TS 38.213 Section 4.1.

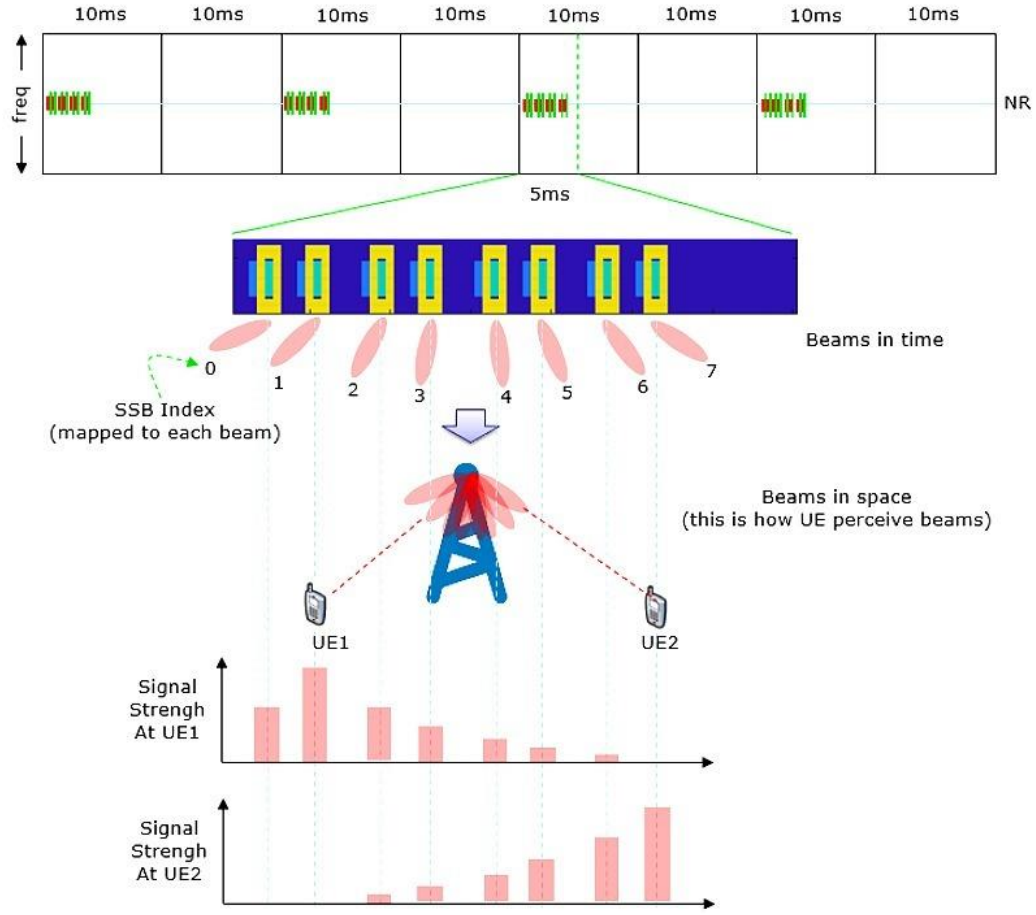

Figure 3.5: Multiple time-multiplexed SS blocks within an SS-burst-set period [69].

This cell search process, without any previously stored information such as carrier frequencies the UE has already camped, starts with the UE scanning all the RF channels searching for one or more SSs positions on the synchronization raster based on the frequency band the UE is performing cell search on. After finding them at a specific Global Synchronization Channel Number (GSCN) associated to each carrier frequency, the UE will then search for the strongest cell, select it, and proceeds to decode the required SI. More information regarding the synchronization raster for each band can be found in TS 38.104 Tables 5.4.3.3-1 and 5.4.3.3-2 [62].

At this stage, both a gNB TX-side and UE RX-side beam sweeping procedure defined in 3GPP TR 38.912 as P-1 BM procedure [56] is carried, consisting of a sequential transmission of the SSBs in different spatial DL directions, where which SSB is mapped to a wider beam for the purposes of

coverage area enhancement and consequently, the higher possibility of synchronization with UEs. An example regarding the beam sweep procedure is exemplified in Figure 3.6, where N transmit beams are transmitted in a way that each one is then received over M receive beams after being transmitted M times from the gNB. For the sake of simplicity, only one SS Burst is generated and processed at the RX M times in the azimuthal plane over a certain time duration, where each interval at the gNB corresponds to an SSB and each interval at the UE corresponds to the SS burst. Additionally, in this scenario, both S3 and U2 beams are highlighted as the theoretically selected beam-pair link.

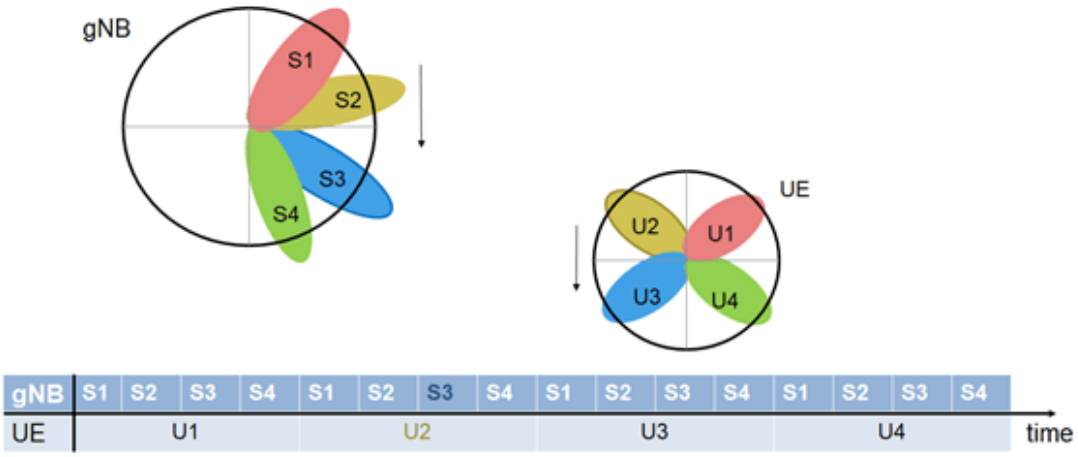

Figure 3.6: Dual beam-sweep at both receiver and transmitter ends (N=M=4) [70].

After the UE acquires an SSB, the PSS is the first specific signal searched by the UE to get the initial system timing and radio frame synchronization when trying to access the cell for the first time. It consists of three possible PSS sequences generated by the application of 3 different cyclic shifts to a sequence of 127 BPSK symbols mapped onto 127 REs. The detection of PSS allows the UE to know the transmission timing of the SSS, corresponding to 1 of 336 possible sequences. Together, these two SSs are used to identify the unique PCI of the discovered cell, a parameter used to distinguish cells on the PHY layer of the 5G RAN, required for DL synchronization and channel estimation [55]. One of the possible 1008 cell ID values can then be simply determined by:

$$N_{ID}^{Cell} = 3 * N_{ID}^{1} + N_{ID}^{2}, \tag{3.1}$$

Where:

- N_{ID}^{1} corresponds to the SSS with the range {0, 1….335}
- N_{ID}^{2} corresponds to the PSS with the range {0, 1, 2}

Thus, an appropriate PCI planning should represent an important role in 5G NR network construction, capable of providing an effective solution to ICI reduction and increased resource utilization over PDCCHs, avoiding collisions, confusions and intercell interference between neighboring cells sharing the same PCI [71].

After PCI identification, the UE can obtain the frequency-domain position of the DMRS in the PBCH to perform channel estimation, measuring the SS-RSRP strength of DMRS of each detected SSB in the search for the strongest one to clearly identify which is the SSB index (i_{SSB}) correspondent to the best suitable RX beam for the UE within the burst it has received. Once the strongest beam has been determined by the UE, it can report the beam measurement results to the UL location mapped to that specific i_{SSB} in gNB via a RA Preamble, known as MSG1, the first of a four-stage RA procedure. This i_{SSB} is also responsible for the association of the different DL beams to different Random-Access Channel (RACH) occasions, enabling RX-side beam-sweeping for the reception of UL RA transmissions as well as DL BF for the RA response.
Having determined the mentioned i_{SSB}, the UE decodes the Master Information Block (MIB) contents, where a combination of System Frame Number (SFN), half radio frame bit, and the frequency domain offset between SSB and the overall RB grid in number of subcarriers (k_{SSB}) parameters allow the acquisition of radio frame synchronization and slot timing so it can determine all or part of the information in the i_{SSB} required for an effective PBCH demodulation [55].

The MIB is broadcasted through the Broadcast Logical Channel (BCCH) mapped to Broadcast Transport Channel (BCH) and carries information needed to acquire the Remaining System Information (RMSI) broadcasted by the network. It also provides more key information to get part of the RMSI needed to access the cell, such as the SIB1 numerology and configuration parameters. On one hand, SIB1 numerology is useful to provide information about the SCS used for SIB1 transmission and information for RA procedures. On the other hand, SIB1 configuration provides information about the search space, corresponding CORESET, and other PDCCH-related parameters that a device needs to monitor for scheduling of SIB1.

Once this information is provided, SIB1, occasionally referred as the RMSI, can be periodically broadcasted over the entire cell area with a 160ms periodicity containing important information required for the UE initial RA procedure. The RMSI needed for a correct UE operation within the network is usually carried out in different SIBs besides SIB1 and can be transmitted on demand to avoid unnecessary periodic broadcasts, leading to enhanced network energy performances. However, these blocks consist of the SI that a device does not need to know before accessing the system. More detailed information about SI acquisition can be found in the following 3GPP specifications:

- MIB acquisition:
  - PSS search and frequency offset estimation in 3GPP TS 38.211, Section 7.4;
  - SSS search and PCI detection in 3GPP TS 38.211 Section 7.4 and 3GPP 38.213, Section 4.1;
  - SS-RSRP measurement in 3GPP TS 38.215, Section 5.1.1;
  - DM-RS search for determination of the LSBs of the SS/PBCH block Index needed for PBCH scrambling in 3GPP 38.211, Section 7.3.3.1;
  - Payload generation, scrambling, transport block CRC attachment, channel coding and rate matching for the PBCH in 3GPP TS38.212, Section 7.1;
  - RRC BCCH-BCH message containing MIB in 3GPP TS 38.331, Section 6.2.1 and MIB message field description in 3GPP TS 38.331, Section 6.2.2.

- SIB1 acquisition:
  - SIB1 message field description with relevant information to access a cell or defining the scheduling of other SI in 3GPP TS 38.331, Section 6.2.2.

3.3.2 Decoding of PDSCH/PUSCH

In the important step where the UE decodes the MIB, it is provided with information regarding the cell barred information state needed to decide whether to continue with a cell selection procedure, concluding the cell search procedure or to restart the process, by finding another 5G cell. If the cell is not barred, the UE will proceed trying to demodulate the PDDCH and blindly search for DCI format messages in the location of the Control Resource Set (CORESET) search space to get the frequency locations of the PDSCH resources to read SIB1 information. For more detailed information about the DCI formats and their correspondent functions and configurations based on different PDCCH payloads can be found in 3GPP TS 38.212, section 7.3.

The PDCCH is responsible to transfer the DCI which is mapped to REs following a certain structure based on Control Channel Elements (CCE), and Resource Element Groups (REG), the unit upon which the search spaces for blind decoding of PDCCH are defined. The PDCCH mapping is done according to the DCI information onto a specific periodic Search space set, with each set mapped onto one specific CORESET, corresponding to a set of time-frequency resources in a specific area of the NR DL Resource grid upon which the UE tries to blind decode PDCCH candidates [55]. It is worth mentioning that is possible to have multiple CORESETs on a carrier and multiple search spaces using the resources in a single CORESET, as illustrated in the Figure 3.7.

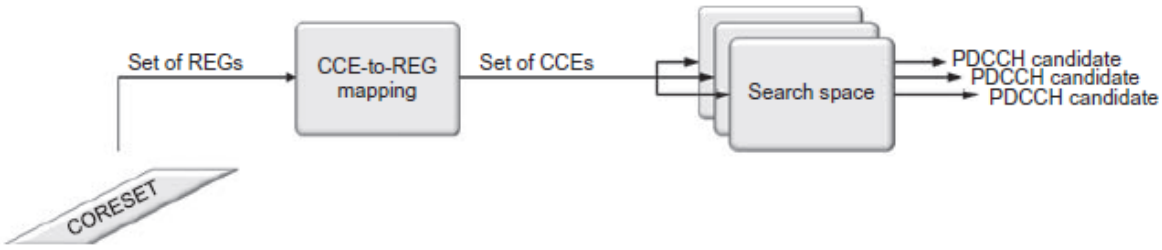

Figure 3.7: PDCCH processing overview [2].

The size and location of the CORESET is configured by the network and can be adjustable within the NR carrier BW to accommodate the UE capabilities, however, for performance purposes in traffic scenarios, a common practice is to locate it at the beginning of the slot for faster scheduling decisions.

Following the determination of the PDSCH configuration using the PCI, the MIB and the DCI already decoded before, the UE gets the remaining SI from the extracted SIB1 such as the PLMN ID, the cell selection parameters and RACH parameters needed for UL synchronization. If this PLMN ID of the network matches with the PLMN ID list available with the UE and the cell selection criterion is fulfilled, the cell selection procedure is accomplished successfully, otherwise, the UE tries to acquire a new NR cell and restarts the process again. A more detailed description of the cell selection process criteria as well as the different cell categories can be found in 3GPP 38.304 sections 5.2.3.2 and 4.5, respectively. A more complete information about cell selection/reselection can also

be found in 3GPP 38.300, Section 5.2, while details on performance requirements for the two processes is presented in 3GPP TS 38.133.

Finally, after the UE and the gNB establish the suitable beam-pair and start to communicate, the gNB sends the RMSI needed for the effective establishment of the connection to the UE. At this point, the system will switch the wider coverage beams to a more UE specific beam centric coverage using beam refinement procedures defined by 3GPP as P2-BM procedures, which are out of the scope for this dissertation, assuring the maintenance of the best selected beam pair quality in RRC connected mode through beam adjustments.

While camped on a cell, the UE regularly performs a cell reselection evaluation process and will reselects onto a more suitable cell, if found. Otherwise, if no suitable cells are found after the initial cell selection, the UE shall find an acceptable cell of any PLMN to camp on while still searching for a higher-quality cell [66]. An overview of all the cell selection steps is presented in the Figure 3.:

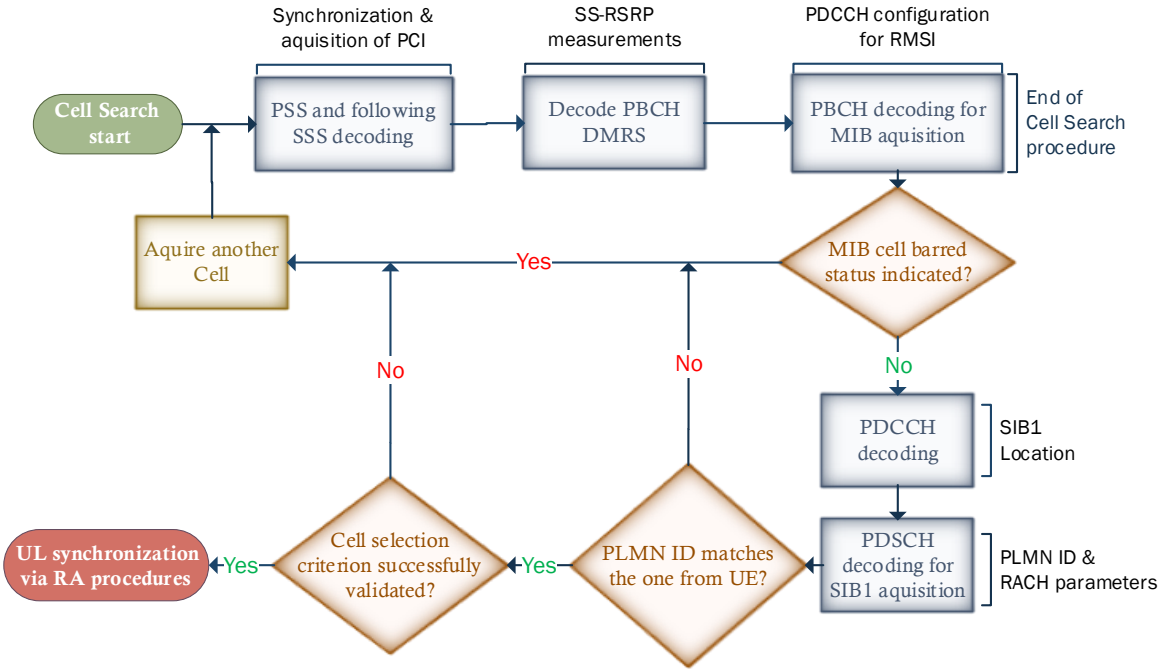

Figure 3.7: Flowchart of the cell selection main steps.

Here below, there is a description with references to 3GPP specifications for a detailed information related to configuration and parameter description needed for the demodulation of the PDCCH and the decoding of DCI:

- PDCCH monitoring occasions determination through a slot and OFDM symbol offset from the location of the SSB detected, described in 3GPP TS 38.213 Tables 13-16 and 13-17;
- CORESET and search spaces configuration according to TS 38.213 Section 13 Tables 13-1 through 13-15A;
- CCE-to-REG interleaved mapping parameters are described in TS 38.211 Section 7.3.2.2;
- CORESET0 BWP with the size of the CORESET, described in TS 38.212 Section 7.3.1.0;
- PDCCH scrambling parameters presented in TS 38.211 Section 7.3.2.3.

Chapter 4

4. Proposed algorithm for beam-pair selection enhancement in IBE stage

In the previous chapters, the importance of employing highly directional arrays in mmWaves spectrum frequencies was discussed. The use of higher frequency spectrum enables the possibility of a higher number of compacted antenna elements at both RX and TX sides due to their reduced individual size, enhancing the transmission BW while BF techniques can be applied to surpass the higher signal attenuations.

In this chapter, a 5G system that generates a NR SS burst, beamforms each of the SSBs within the burst to sweep over both azimuth and elevation directions, transmits this beamformed signal over a spatial scattering channel, and processes this received signal over the multiple receive-end beams is implemented. Initially, some tools used for the system simulation are presented, followed by a more in-depth description of the generated signal burst by the TX, the channel and RX models, as well as its working description, emphasizing the BF steps following 5G NR standards.

Finally, a proposed beamforming based on SSS angle estimation (BSAE) algorithm is designed and implemented in a simulation environment for subsequent BER performance analysis focusing the main specified 3GPP P-1 BM DL procedures for the NR IBE stage. The primary goal comprises the enhancement of the acquisition of a suitable beam-pair link, i.e., a gNB used beam paired with one RX beam at the UE, improving the overall system efficiency.

4.1 Related works for beam-pair selection enhancement

This subsection presents a state-of-art regarding the main topic of this dissertation. Although a set of 3GPP specifications have been already defined for the suitable beam pair selection of the highly directional beamformed transmissions required to enable the communication in the mmWave frequency bands, there is a lot of flexibility in how the required procedures are implemented.

To address the reliance on directional BF and its inherent complications in the initial cell search stage in scenarios where many UEs and BSs must cooperatively search over a large angular directional space to locate a suitable path to initiate communication, the authors of [72] proposed a directional cell discovery procedure, where BSs periodically transmit SSs in both time-varying random and omnidirectional directions to scan the angular space. The results, derived from actual field measurements for both single and multipath channels, showed that omnidirectional transmissions of SSs have much better performances than random angular search, in both digital and analog cases. Additionally, it was also concluded that digital BF offers significantly better performances than analog BF even when digital BF uses very low quantification to compensate for

the additional power requirements, suggesting that a low rate per antenna digital BF design with an appropriate search algorithm may be a better choice for initial cell search, while hybrid or analog BF should be used for the remaining communications once the connection has finally been established in both directions.

An extension to the previous work is presented in [73] where the authors proposed several different SA mmWave design options for the directional search in the IA procedure, comprising both the synchronization phase, where the UE discovers the BS and the RA phase, where the BS detects the RA request from the UE. A further comparison between the different designs considering different scanning and signaling procedures to evaluate access delay and system overhead was made for both realistic LoS and NLoS scenarios. The obtained results demonstrated significant benefits of low-resolution fully digital architectures in comparison with single stream analog BF, not only offering significantly improved data rates and lower data plane latency but also significantly reduced control plane latency. Furthermore, practical evaluations point out that the short SSs duration needed for the directional transmissions to perform as well as omni-directional ones may be too short for practical implementations.

To similarly address the high overhead problem for the required directional link establishment which restricts the mmWave high throughput capabilities, beam-width scalability and mobility support, the authors of [74] designed and implemented an assisted beam-pair selection algorithm to remove in-band overhead on LoS scenarios, coupling mmWave architectures with legacy sub-6GHz bands while using out-of-band direction interference to establish communication. The experimental results obtained from the passively direction estimates of the pairing nodes without incurring in any additional protocol overhead demonstrated that the algorithm achieves on average 97.8% accuracy for direction estimation when 5 or more antennas are used at the detection band. Additionally, it can also detect unobstructed direct path conditions with an accuracy of 96.5% while reducing the BF training overhead by 81% for highly directional transceiver with 7-degree beam width.

More related work focusing on the mitigation of the total duration of IA directional search is presented by the authors of [75] and [76], revisiting different techniques of exhaustive and iterative beam search to propose a novel hybrid training method, where the BS performs wide beam search in the first stage while the UE will perform reverse training according to the best wide beam decided on the first stage. These more complex implementations are based on the initial transmission of SSs in few directions over wide beams, which are subsequently refined until the communication is satisfactorily directional. The simulated results revealed that the designed hybrid training method reduces searching delays while providing similar access error probability as iterative search without much more UE power consumption.

There is also some additional work based on several sources of side-information that successfully help the establishment of the mmWave links with substantially reduced training overheads for the beam-selection stage. They include the use of spatial information retrieved from sub 6GHz frequency bands in an analog mmWave system, proposed by the authors of [77], the leveraging of vehicle's position information along with past beam measurements to rank desirable pointing directions that can reduce the required beam training to a small set of pointing directions, proposed by the authors of [78], and also a novel framework of 3D scene based beam selection information for mmWave communications, proposed by the authors of [79]. This last work relies only on the environmental

data and deep learning techniques of neural networks used alongside image processing techniques to improve the suitable beam selection. The proposed approach can predict the optimal beam pair for any point in the current cell and can further work for a new environment with the same type of building distributions. The simulated results showed a reduction of the beam-training overhead and a higher beam selection accuracy, clearly demonstrating the advantage of exploring 3D reconstruction techniques for beam selection methods to avoid severe overheads by using expensive auxiliary devices, such as Radar or Light Detection And Ranging (LIDAR).

Moreover, the authors of [80] proposed a BM strategy based on a conjunction of beam orientation information retrieved from on-board sensors at the UE with RSRP measurements to improve beam determination accuracy and achieve reduced power transmission values, allowing for a considerable higher UE battery life duration. In this algorithm, the source of side-information is available at the UE and thus, it requires no additional signaling overhead to be used for the optimal transmit and receive beam pair predictions. Exhaustive simulations accounting realistic channel models, practical beam patterns and many UE movements and rotation speeds without additional transmission of signaling overheads were performed and the obtained results showed a significant a great improve in the beam prediction accuracy and power loss reduction triggered from the sub-optimal beam pair selection in BM procedures.

The authors of [70] present a beam pair selection algorithm which deploys BM procedures at both the gNB and the UE ends of a NR system to acquire a set of beam pair links using SSBs transmitted as a burst in the DL direction. In this algorithm, described in Algorithm 1 below, a set of beamformed SSBs is swept over both azimuth and elevation directions to be further transmitted over a spatial scattering channel and consequently processed over multiple receive-end beams. Afterwards, the RSRP values for each correspondent transmit-receive beam pair combination are measured and the beam pair link with the maximum RSRP value is chosen as the most suitable one to establish connection.

Algorithm 1: Beam-Pair Selection based on RSRP maximization Algorithm

For ID_{TX}=1, ..., $N_{TXBeams}$ (Number of Transmit end Sweep beams)
    Generate weights for steered beam directions and apply them to each SSB
End
For ID_{RX}=1, ..., $N_{RXBeams}$ (Number of Receive end Sweep beams)
    Generate weights for steered beam directions and apply them per receive element
    For ID_{TX}=1, …, $N_{TXBeams}$ (Number of Transmit end Sweep beams)
        Measure the RSRP for each Beam-pair
    End
End
Determine the best beam-pair link based on the maximum RSRP value

Finally, contrasting with the work mentioned above, where the proposed algorithm only choses the beam pair that maximizes the RSRP while neglecting the information contained in all the other

beams, the proposed algorithm contained in this dissertation performs the beam pair selection based on information relative to all the beams without the addition of significant complexity to the overall system since the processing of all the candidate beam pairs were already done. This optimization is accomplished by a beam angle refinement process at the UE side using the SSSs present in each SSB, focusing the application of BM techniques to the subsequent enhancement of the overall NR system performance. Later in this chapter, a performance evaluation of the beam pair selection based on RSRP maximization is going to presented along with the comparison to the proposed enhanced beam-pair determination algorithm based on SSSs angle estimation.

4.2 System Design

In this section, a more detailed description of the TX, channel and RX model considered for the application of BM procedures at both the TX and RX-side directions during IA is presented. The simulated system uses both the 5G toolbox and the Phased Array System Toolbox. The first one provides 3GPP-standard compliant functions and reference examples useful for modelling and simulation of a 5G NR end-to-end communication system, since the DL physical channels and signals creation for transmission and reception of DCI messages to the DL synchronization, demodulation, and further decoding of a live gNB signal at the UE. On the other hand, the phased array system toolbox provides the necessary algorithms for enabling BF techniques with electronically steerable antennas, allowing the simulation of multipath fading environments to evaluate the performance of the employed BF AAs.

An overview of the main processing stages required for the dual-end beam sweeping procedure at both the gNB and the UE ends, along with the main BM steps for an effective beam-pair establishment and maintenance are highlighted in red color in the Figure 4.1:

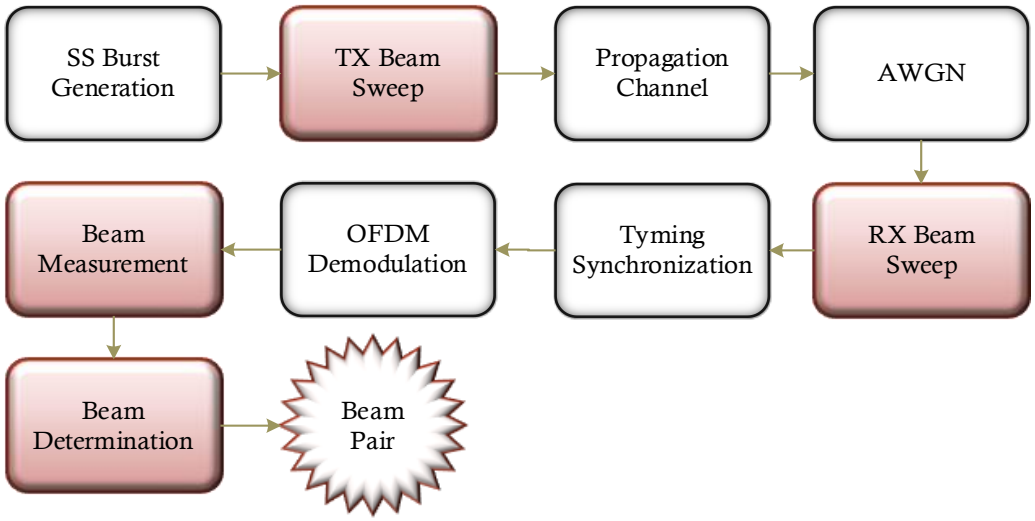

Figure 4.1: Main processing simulation steps.

4.2.1 Transmitter Model Description

The TX, equipped with N_{TX} antennas, is responsible for the generation and transmission of a DL waveform which will be subject to some BM techniques used in the IA procedure, where a connection is established between the gNB and the UE. After a SS Burst have been generated and configurated carrying the MIB and the DMRS for the PBCH demodulation, every SSB is then beamformed within the burst and swept over both azimuth (Δ_θ) and elevation ($\Delta_\emptyset$) specified directions within the SS Burst periodicity. The SS Burst spectrogram is presented in the following Figure 4.2:

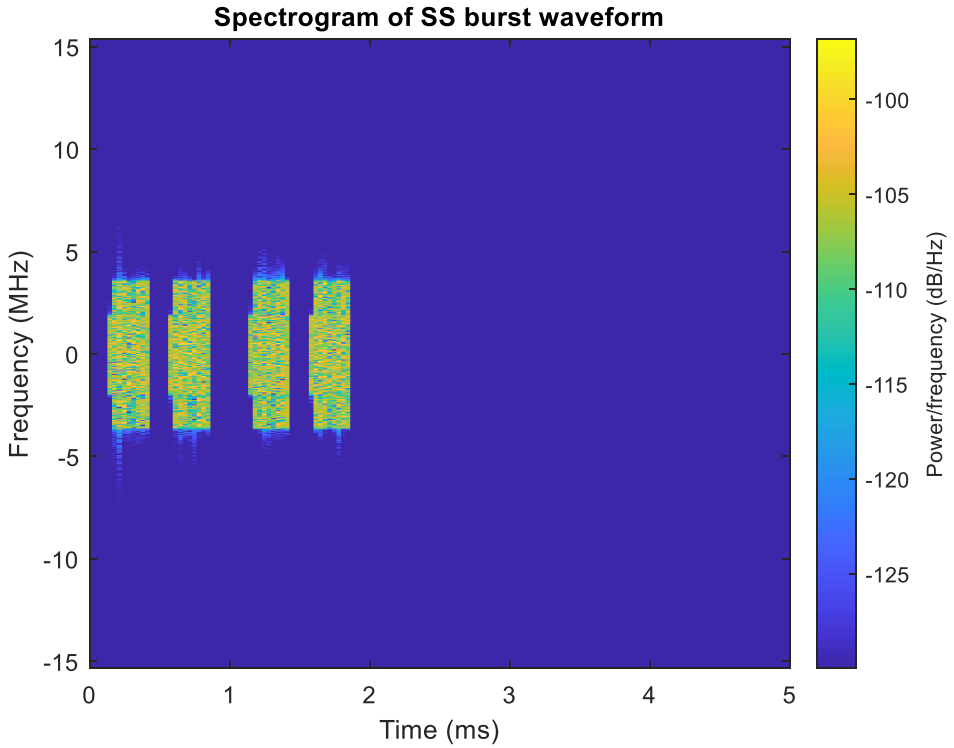

Figure 4.2: Spectrogram of the generated SS Burst.

This beamformed signal is then transmitted over a spatial scattering channel, which will be presented in the following section, and then processed over each one of the multiple receive-end beams in a dual-end beam sweeping process.

4.2.2 Channel Model Description

A spatial scattering MIMO channel is used, modeling a LoS multipath propagation channel where the transmitted array radiated signals are reflected from multiple scatterers to the receiver. This channel model applies free space path loss and specifies the locations for both the BS and UE as [x,y,z] coordinates in a Cartesian system, consisting of a Uniform Rectangular Array (URA) and an Uniform Linear Array (ULA) with isotropic antenna elements at the TX and RX, respectively.

Additionally, to simulate the noise in the actual propagation medium, distributed and uncorrelated additive white gaussian noise (AWGN) is added to the transmitted signal [81].

The spatial scene illustrating a combined view of the channel scatterers along with the TX and RX determined beams is presented in the Figure 4.3:

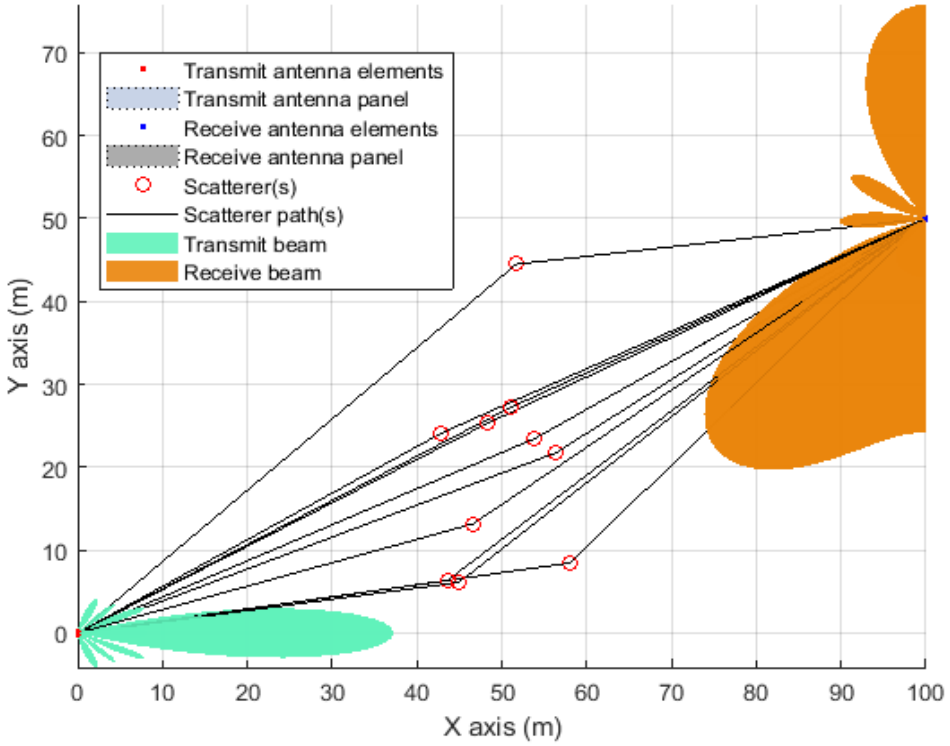

Figure 4.3: Spatial scattering scene.

Additionally, the directivity patterns related to both the TX and RX are shown in the following Figure 4.4:

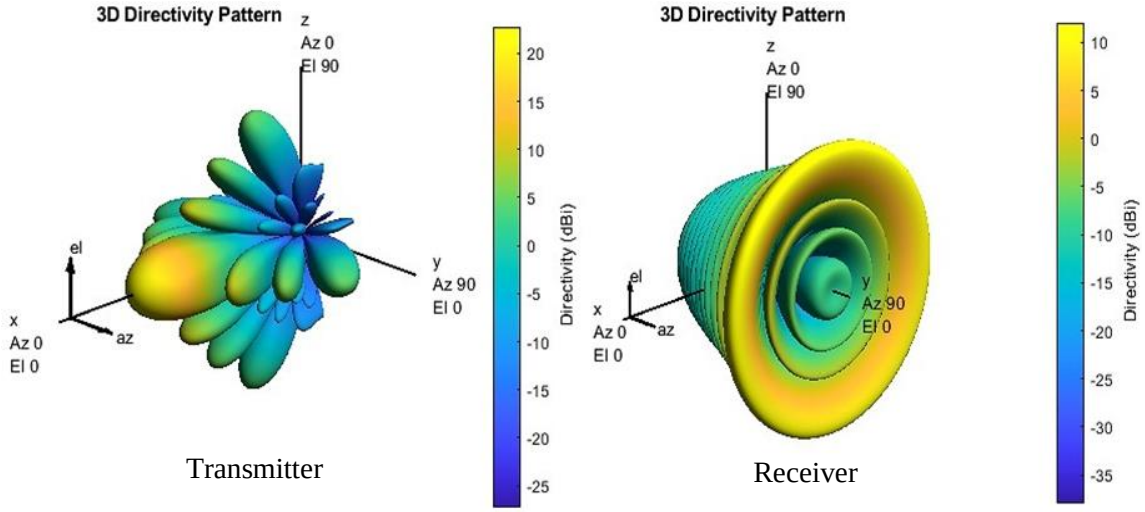

Figure 4.4: Selected Transmit/Receive Array response pattern.

4.2.3 Receiver Model Description

The RX is responsible for several needed synchronization and demodulation processes of the received waveform to determine the System Frame Number (SFN) and the PCI to decode the MIB, providing the required initial SI for blind decoding of DCI in a PDCCH. The RX will further use DCI to configure the PDSCH demodulator, decode the DL-SCH and finally recover the Transport Block (TB) information.

The following Figure 4.5 presents a more detailed diagram of the received signal processing steps inside the RX to perform the acquisition of frame synchronization and the further required cell search and selection procedures before the UE can communicate with the network. The remaining of this subchapter will cover the discussion of the received signal demodulation process complemented with simulated images from the starting PSS search procedure until the effective DL-SCH decoding stage.

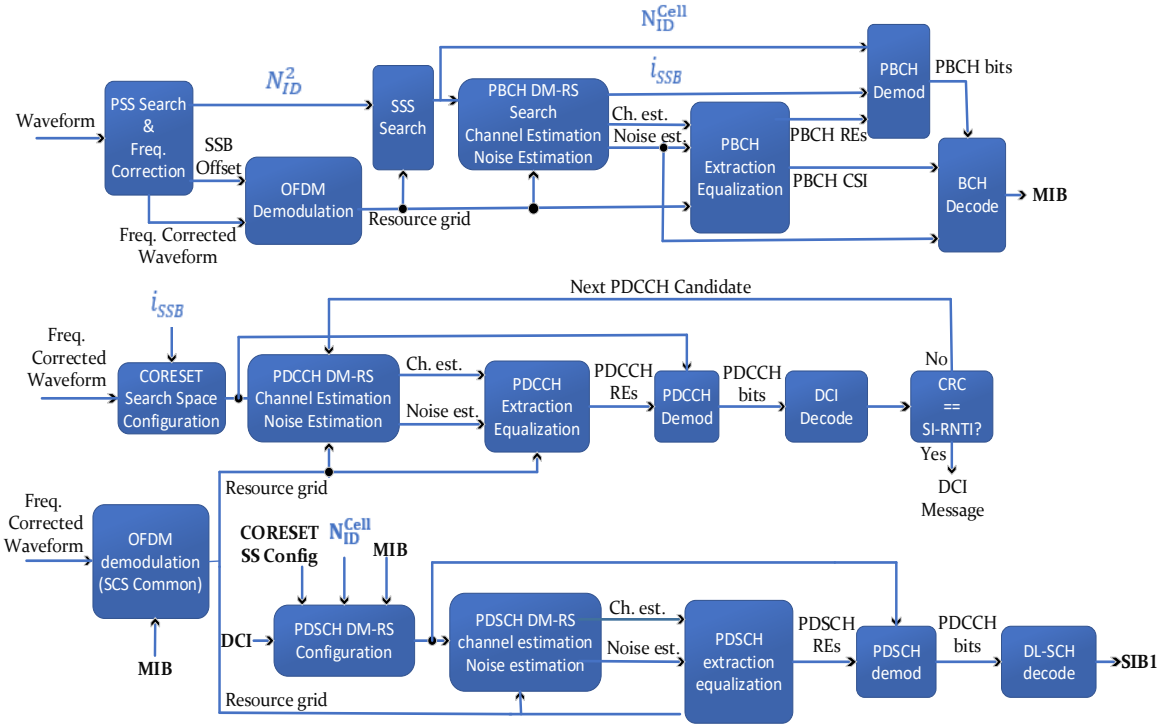

Figure 4.5: Detailed block diagram of the receiver processing steps [82].

Additionally, Figure 4.6 shows the spectrogram of the received waveform:

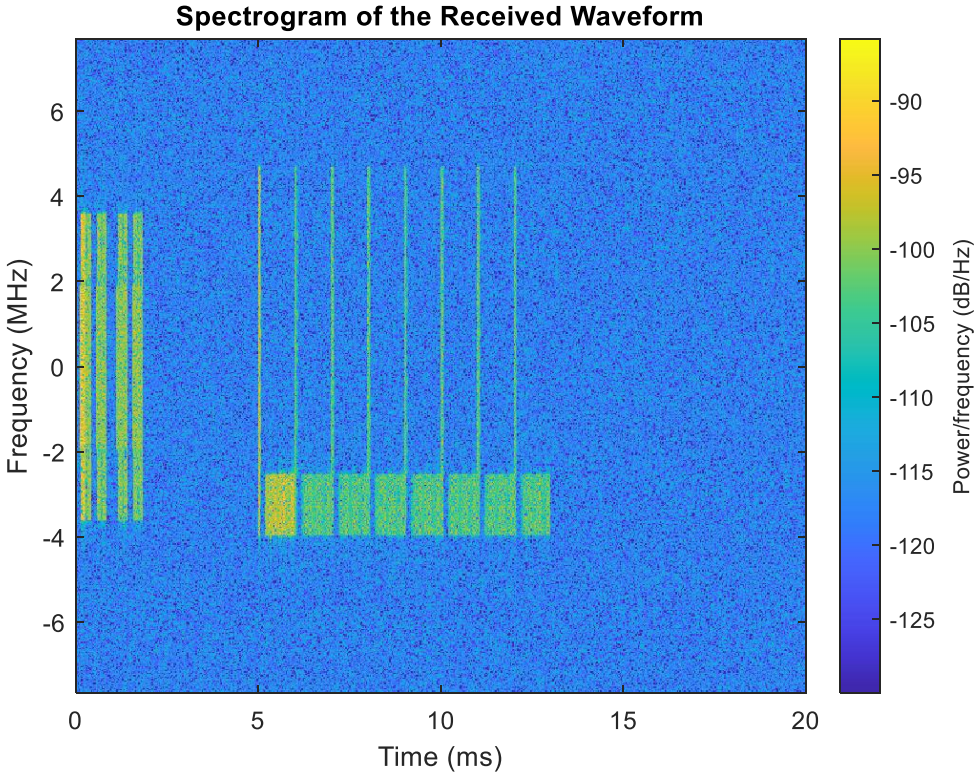

Figure 4.6: Spectrogram of the received waveform.

After the signal transmission by the gNB, the UE starts a synchronization procedure with the TX performing PSS search and coarse frequency offset estimation following these steps:

- Frequency shifts the received waveform with a candidate frequency offset which are spaced half subcarrier apart.

- Correlate the frequency-shifted received waveform with each of the three possible N_{ID}^2 sequences centered in frequency and extract the strongest correlation peak, providing a measure of coarse frequency offset (coarse $\triangle_f$) with respect to the center frequency of the carrier and also the indication of the PSS sequence that has been detected in the received waveform at the time instant of the best channel conditions, as shown in Figure 4.7.

- Do an estimation of frequency offsets lower than half subcarrier by correlating the CP of each OFDM symbol in the SSB with the corresponding useful parts of the OFDM symbols resulting in a correlation phase proportional to the frequency offset in the waveform.

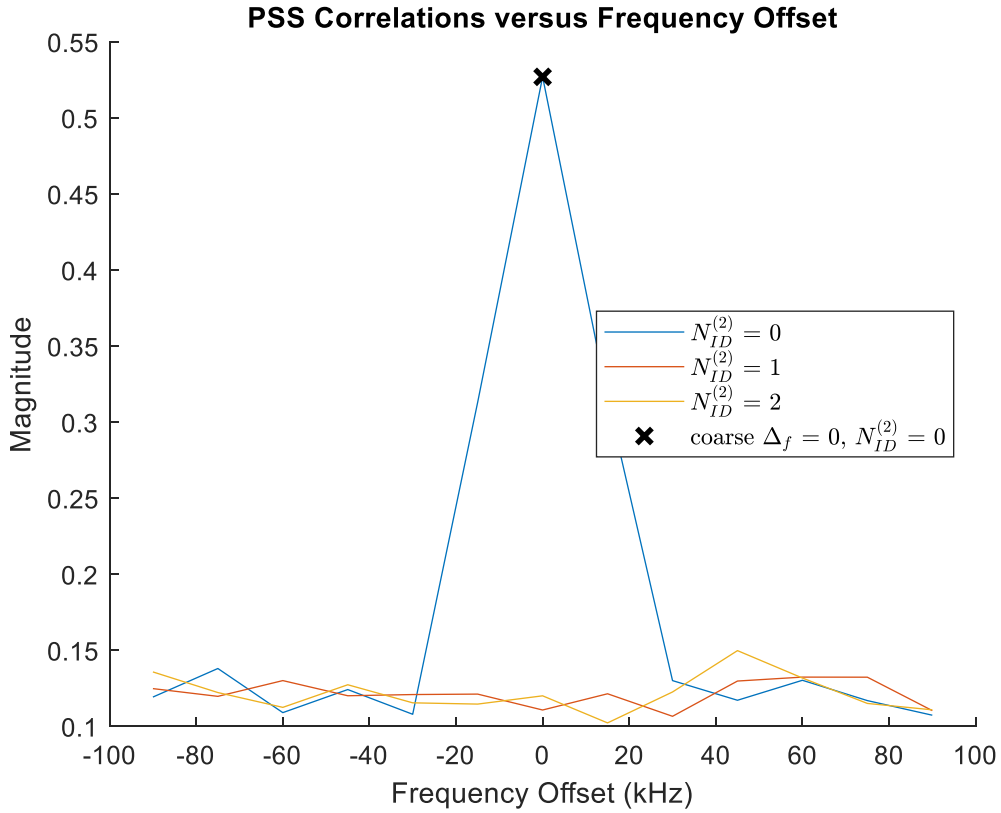

Figure 4.7: PSS Correlations vs. Frequency Offset for N_{ID}^{2} determination.

Having found the strongest PSS sequence, i.e., position of the 1st symbol in the radio frame, the RX can proceed with the time synchronization process by estimating the timing offset of the strongest SSB due to the content of the reference grid, for frequency offset correction purposes. This is an important step that allows the UE to assume that the center frequencies of both the reference PSS sequence and the one from the received waveform are aligned and thus, the OFDM demodulation of the synchronized waveform and the extraction of the strongest SSB can take place.

For an effective PCI detection required for PBCH DM-RS and PBCH processing, the RX also extracts and correlates the resource elements associated to the SSS with each of the possible 336 sequences generated locally to obtain the strongest SSS sequence (N_{ID}^{1}), as illustrated in Figure 4.8.

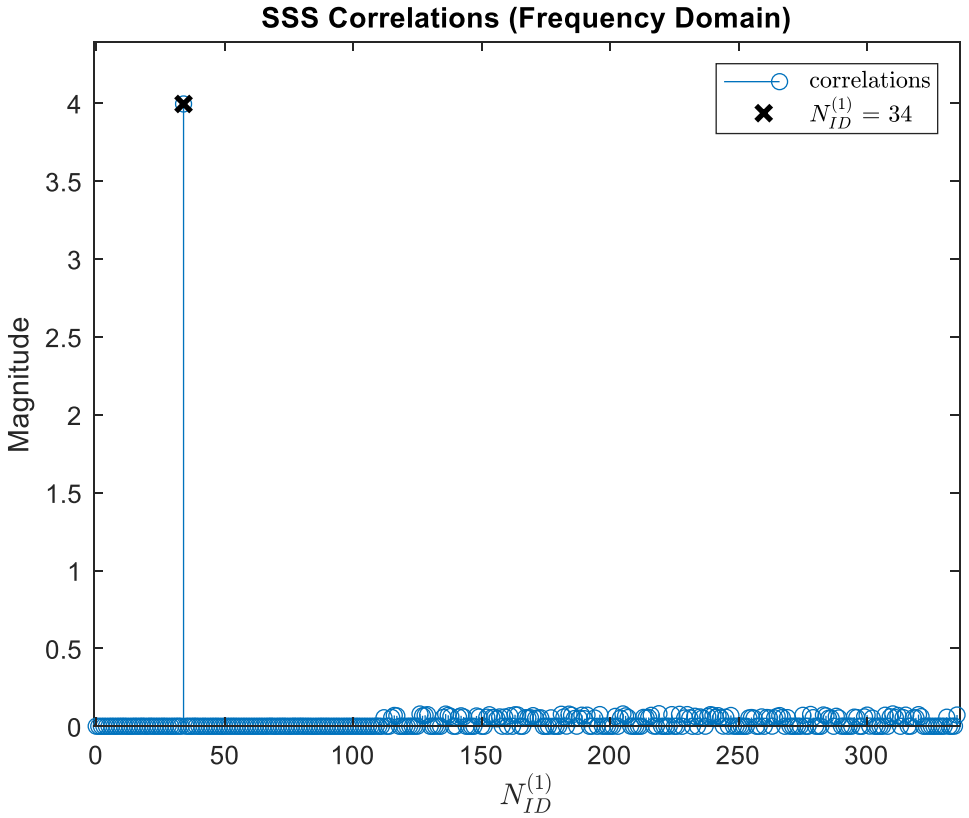

Figure 4.8: N_{ID}^{1} determination to obtain cell identity.

After having detected the PCI using (3.1) the UE will determine the frequency-domain position of the DM-RS candidates in the PBCH according to the 'case B' SSB transmission pattern used for simulation purposes in this dissertation. At this phase of the cell search procedure, the UE also performs both channel and additive noise estimations for the entire SSB based on the SSS and PBCH DM-RS detected in the previous steps. This additional use of the SSS for the determination of the impact of the propagation channel is possible due to the location of SSS in the PBCH, leading to similar propagation channel experienced for both signals. Afterwards, the respective PBCH DM-RS index with the best SNR value is subsequently used to determine the LSBs of the i_{SSB} required for PBCH scrambling initialization, as shown in Figure 4.9.

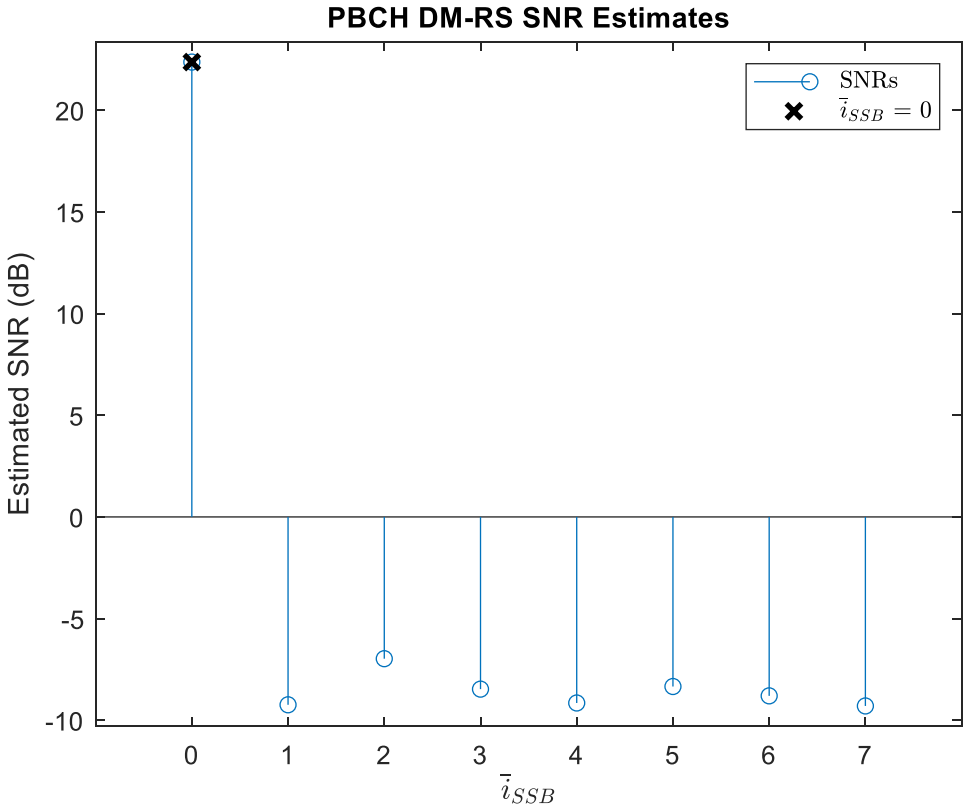

Figure 4.9: Selected i_{SSB} for the highest SNR value.

Once the UE has finally obtained the PCI and completed the channel and noise estimations mentioned before, it will proceed with Minimum Mean Square Error (MMSE) equalization, where the equalized PBCH symbols presented in Figure 4.10 are then demodulated and descrambled to give bit estimates of the coded transport BCH block, which will be later weighted with CSI from the MMSE equalizer for PBCH decoding.

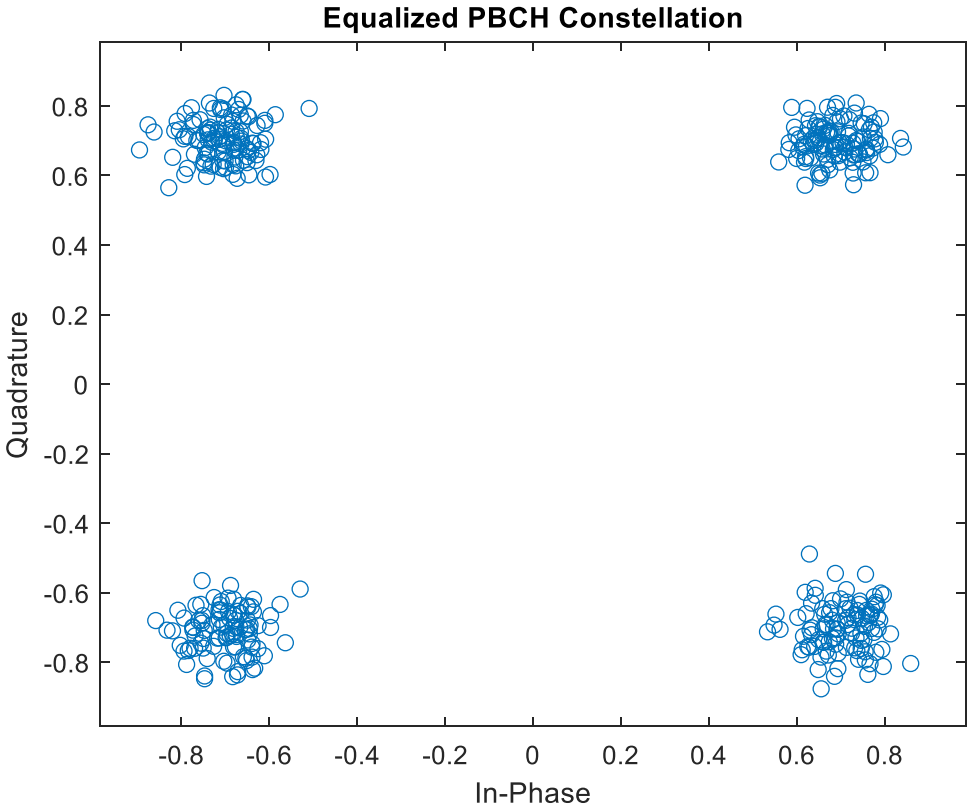

Figure 4.10: Received PBCH constellation after equalization.

After the cell search procedure has been concluded with the parsing of the decoded BCH TB bits into the MIB message, the UE will then use a common SCS value and determine a minimum BW supporting CORESET 0 to OFDM demodulate the frame containing the detected SSB. However, before the OFDM demodulation process, the already aligned center frequencies of the OFDM resource grid and the SS burst need to be aligned with the center frequency of the CORESET 0 through a frequency shift determined by k_{SSB} to assure that the control and data channels are also aligned in frequency with their CRB raster.

The OFDM demodulated received resource grid with the highlighted strongest RB is presented in the following Figure 4.11:

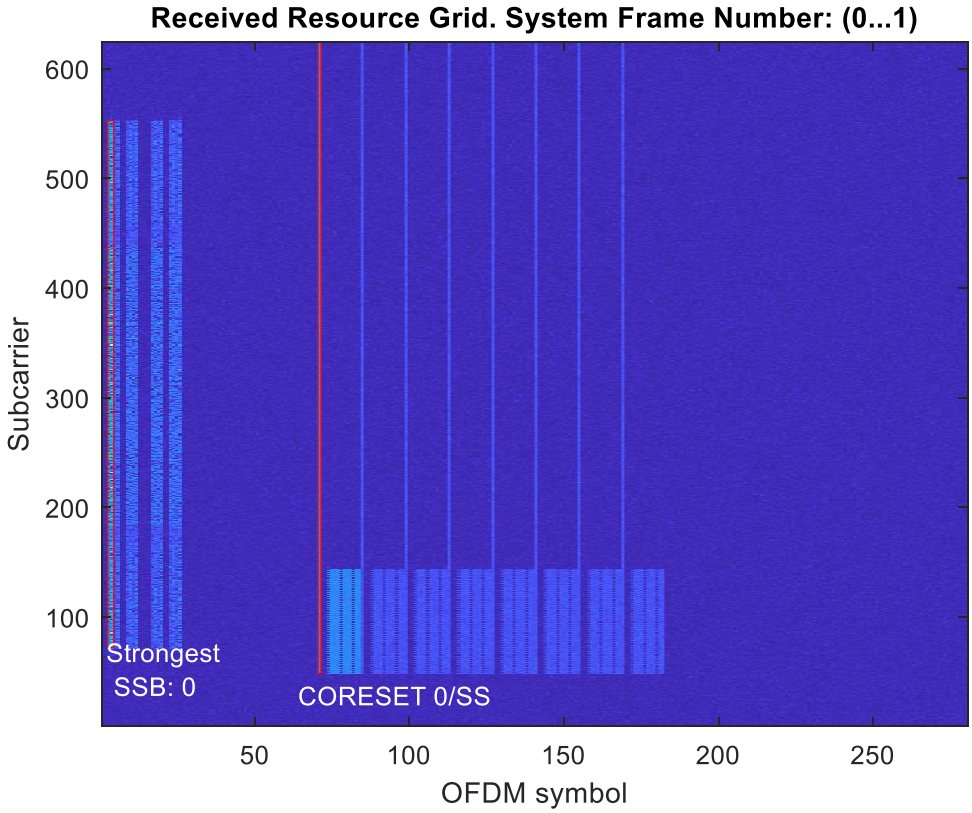

Figure 4.11: OFDM resource grid and the highlighted chosen SSB.

After the OFDM modulation on full BW, the UE will perform PDCCH demodulation and blindly search for DCI format messages in the location of the CORESET Search Space. The UE will then blind decode the received PDCCH symbols by monitoring all PDCCH candidates for every aggregation level (contiguous control channel elements upon which the PDCCH is transmitted), as shown in Figure 4.12.

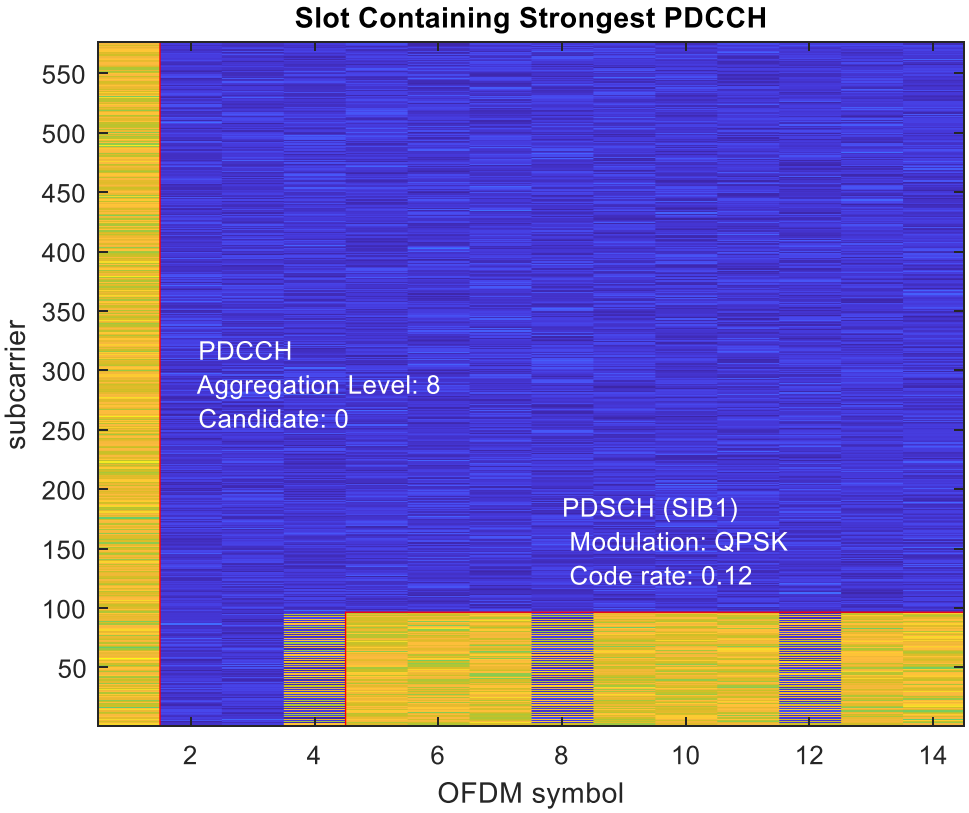

Figure 4.12: OFDM grid of the slot containing the strongest PDCCH.

For finally being able to recover the first SIB1, the RX needs to determine the PDSCH configuration using the cell ID, the MIB and the DCI already decoded before. Additionally, the PDSCH channel estimation and equalization using PDSCH DM-RS also occurs, where the impacts of a possible carrier mismatch in symbol phase compensation and channel estimation are reduced by OFDM waveform demodulation with a set of carrier frequencies over a search BW around the carrier center frequency that will finish when DL-SCH decoding succeeds, or the last search frequency has been reached.

Lastly, after the demodulation of the PDSCH symbols, the UE can perform the effective decoding of the DL-SCH.

4.2.4 Proposed Beamforming based on SSS angle estimation Algorithm

An illustration of the BSAE algorithm concept is presented in the following Figure 4.13:

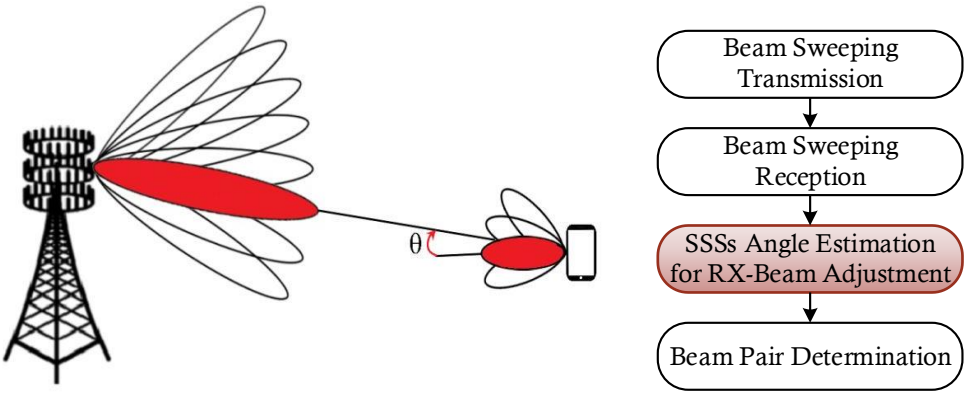

Figure 4.13: BSAE algorithm concept.

To achieve better system performance levels in the effective decoding of transmitted information, the UE can additionally use the SSS in combination with DMRSs to determine the impact of the propagation channel and then apply the inverse to the PBCH payload before the decoding attempt since these two signals experience similar propagation channels effects. However, the RX processing is carried out after ADC conversion and thus, to efficiently perform better Rx beam angle adjustments, an equivalent channel estimation of the analog part is required. Considering a DL system with a BS equipped with N_{tx} transmit antennas as well as a single user equipped with a single RF chain and N_{tx} receive antennas, the received SSS signal $\tilde{d}_{k,s} \in \mathbb{C}$ at the *k*th subcarrier for the *s*th analog beam at the UE, is given by:

$$\tilde{d}_{k,s} = \mathbf{w}_{a,s}^{H}\mathbf{H}_k\mathbf{f}_a d_k + \mathbf{w}_{a,s}^{H}\mathbf{n}_{k,s}, \tag{4.1}$$

where the $d_k \in \mathbb{C}$ is the transmitted SSS at the subcarrier *k* while the $\mathbf{f}_a \in \mathbb{C}^{N_{tx}}$ and $\mathbf{w}_{a,s} \in \mathbb{C}^{N_{rx}}$ parameters model the analog beam at the BS and the UE, respectively. Additionally, $\mathbf{H}_k \in \mathbb{C}^{N_{rx}\times N_{tx}}$ is the frequency domain channel at the subcarrier *k* and the $\mathbf{n}_{k,s} \in \mathbb{C}^{N_{rx}}$ parameter denotes the zero mean Gaussian noise, with variance σ_n^2 .

Having the transmitted and received SSSs the equivalent channel estimation in the digital part based on the SSSs can be estimated by:

$$\tilde{\mathbf{h}}_{eq,k,s} = \tilde{\boldsymbol{d}}_{k,s}\boldsymbol{d}_k^{-1}, \tag{4.2}$$

At this point, the equivalent channel estimated in (4.2) contains the needed analog counterpart estimation. Considering $\mathbf{W}_a = [\mathbf{w}_{a,1}, \ldots, \mathbf{w}_{a,S}] \in \mathbb{C}^{N_{rx}\times S}$, where *S* is the number of beams in the beam sweeping procedure, $\mathbf{N} = [\mathbf{n}_1 d_k^{-1}, \ldots, \mathbf{n}_S d_k^{-1}] \in \mathbb{C}^{N_{rx}\times S}$, and $\tilde{\mathbf{h}}_{eq,k} = [\tilde{h}_{eq,k,1}, \ldots, \tilde{h}_{eq,k,S}]^T \in \mathbb{C}^S$. Then, from (4.2), we have:

$$\tilde{\mathbf{h}}_{eq,k} = \mathbf{W}_a^H\mathbf{H}_k\mathbf{f}_a + \mathbf{W}_a^H\mathbf{N}, \tag{4.3}$$

Therefore, $\mathbf{W}_a$ is a square matrix, with $\mathbf{w}_{a,1}, \ldots, \mathbf{w}_{a,S}$ selected to be an invertible matrix and we can estimate the channel in analog part, $\mathbf{h}_{a,k} = \mathbf{H}_k \mathbf{f}_a \in \mathbb{C}^{N_{rx}}$ by:

$$\tilde{\mathbf{h}}_{a,k} = (\mathbf{W}_a \mathbf{W}_a^H)^{-1} \mathbf{W}_a \tilde{\mathbf{h}}_{eq,k}. \tag{4.4}$$

Hence, the receive beamformer, $\bar{\mathbf{w}}_a \in \mathbb{C}^{N_{rx}}$ can be found by solving the following problem:

$$\begin{gathered} \bar{\mathbf{w}}_a^H = \arg_\theta \max \left\| \bar{\boldsymbol{w}}_a^H(\theta)\, \tilde{\mathbf{h}}_{a,k} \right\|, \\ \bar{\mathbf{w}}_a^H \in \Omega_a \end{gathered} \tag{4.5}$$

where Ω_a is the set of feasible vectors and $\bar{\boldsymbol{w}}_a^H(\theta)$ is the array response vector for angle θ.

Compared to the beam-pair selection based on RSRP maximization algorithm that performs a dual end beam sweep with pre-configured beam directions for the subsequent suitable beam pair selection, the proposed BSAE algorithm described in the following Algorithm 2 incorporates the previous described operations of channel estimation in the digital domain without adding much complexity to the main system since the channel estimation process was already performed. At this point, it is important to remove the effects of the analog processing for the further use of a combination of channel estimations to perform the equivalent channel propagation matrix estimation without the analog processing effects. This matrix can then be used for a further metric evaluation of different steering angle vectors to determine the one that maximizes the RSRP and finally compute a best suitable adjusted beam at the RX end.

Algorithm 2: Proposed BSAE Algorithm

For ID_{TX}=1, ..., $N_{TXBeams}$ (Number of Transmit end Sweep beams)
  Generate weights for steered beam directions and apply them to each SSB
End
Calculate Rx Beam Angle Sweeping values between Azimuthal limits
For ID_{RX}=1, ..., $N_{RXBeams}$ (Number of Receive end Sweep beams)
  Generate weights for steered beam direction and apply them to each receive element
  Extract the received SSSs
  Get SSSs symbols for the PCI
  Channel propagation matrix estimation in the digital part based on SSS (4.2)
End
Channel propagation matrix estimation in the analog part based on SSS (4.4)
Extract the optimized Rx Beam Angle considering the optimization problem (4.5)

4.3 Performance Results

In this section, the simulated performance results of the described beam pair selection scenarios are presented in terms of correct MIB, DCI and DL-SCH decoding percentages alongside with the BER metric, presented as a function of E_b / N_0, where E_b is the average bit energy and N_0 is the one-sided noise power spectral density. The QPSK is the modulation scheme adopted in this section and the Transport Block Size (TBS) is 176.

The simulation was done for three different algorithms where the vectors specifying the antenna element array sizes are composed by a two-element row vector size specifying the number of antenna elements in the rows and columns. A URA vector specifying the antenna element array sizes is used when both values are greater than one while a ULA is assumed if any of the value is one.

The three different simulated algorithms are:

- **1**: Beam-pair selection based on RSRP maximization algorithm;
- **2**: Optimum beam-pair angle selection algorithm, for comparison purposes;
- **3**: Proposed BSAE algorithm.

The considered optimum beam-pair selection algorithm corresponds to the case where the real channel matrix is used to compute the optimal RX angle, however, since this matrix is not known in practical implementations, this algorithm is not feasible in real-time scenarios.

In each simulation, for the sake of simplicity, a single cell scenario with only one BS and one UE was considered for both FR1 and FR2 mode operation (normal CP values). The considered transmit array is an URA with N_{Tx} =64 whereas the receive array was employed with an ULA type configuration with N_{Rx} =16. Additionally, 8 SSBs per SS burst (L) for the frequency mode operation.

A more complete list of system parameters commonly used for the three algorithms mentioned above are presented in Table 4.1:

Table 4.1: Simulation Parameters.

	Parameter	Value
Main	Δ_f	30 kHz (FR1); 120 kHz (FR2)
	N	10000
	L	8
	f_c	3.5 GHz (FR1) ; 28 GHz (FR2)
	$BW_{Channel}$	100 MHz (FR1); 400 MHz (FR2)
Transmitter	Δ_θ	[-60;60]
	$\Delta_\emptyset$	[-90; 90]
	f_s	15.36 MHz (FR1); 61.44 MHz (FR2)
	T_{SS}	20ms
	N_{Tx}	64
	Array configuration	URA
Channel	N_{cl}	10
	TX position	[0;0;0]
	RX position	[100;50;0]
Receiver	Δ_θ	[-100;100]
	$\Delta_\emptyset$	[-90;90]
	N_{RX}	16
	Array configuration	ULA

4.3.1 FR1 operation mode

The following Figure 4.14 to Figure 4.16. illustrate the comparison of the different decoding percentages of the DL PHY channels of the three algorithms referred above for the FR1 operation mode. Despite the lower effective PBCH decoding throughput of the designed BSAE algorithm, we can verify an enhancement in the DL-SCH decoding percentages, where the worst performance of the beam-pair selection algorithm based on RSRP maximization is noticeable with almost all TBs only successfully decoded above E_b / N_0= 0 dB. Additionally, the BSAE algorithm achieves sensibly 100% throughput percentage for values higher than E_b / N_0= -12 dB, which corresponds to a 12 dB performance improvement gain. Comparing the DL-SCH decoding throughput between the proposed and an optimal beam pair determination algorithms, it is still possible to observe similar performances.

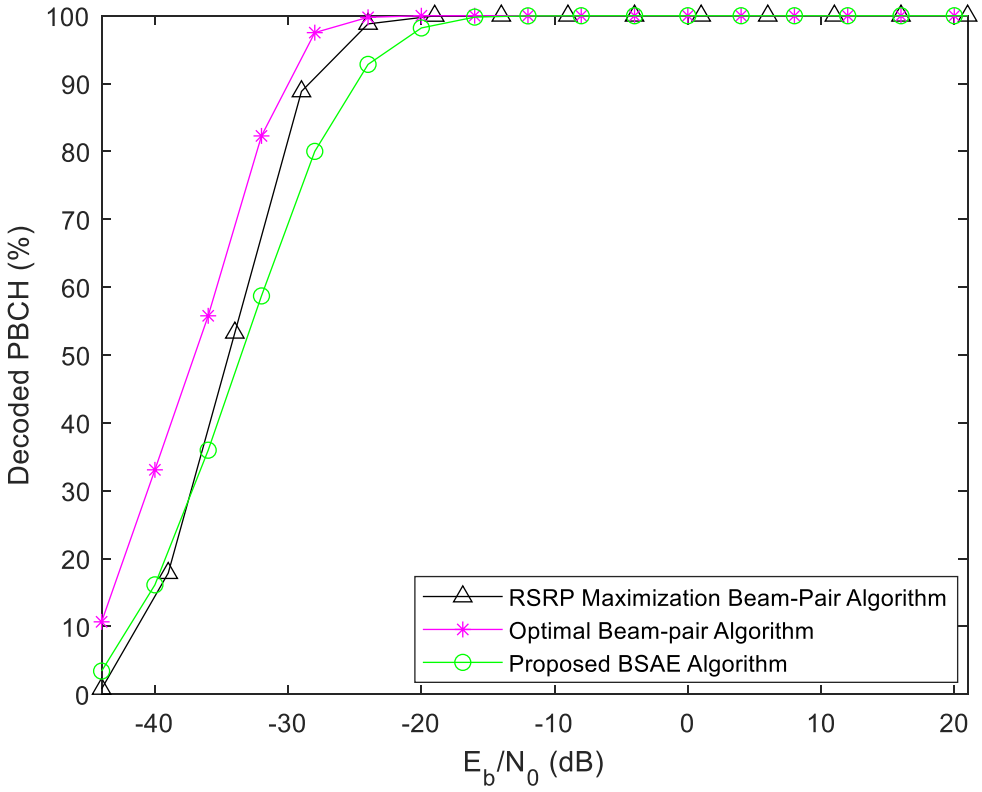

Figure 4.14: Decoding percentage of PBCH for FR1.

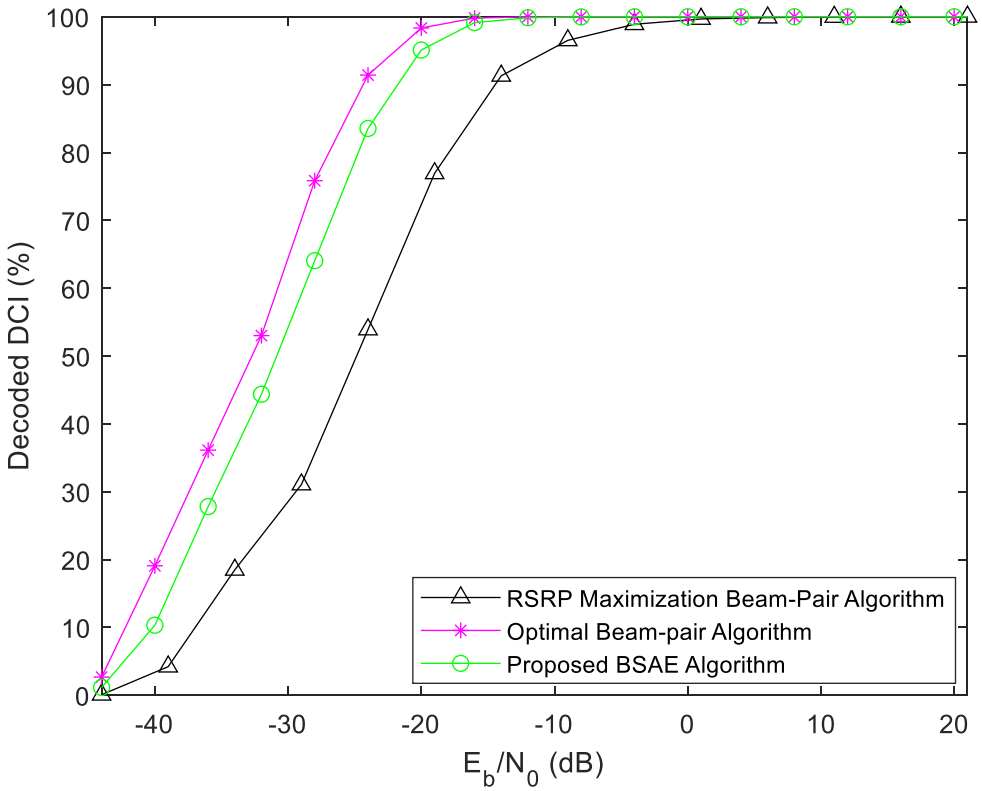

Figure 4.15: Decoding percentage of PDCCH for FR1.

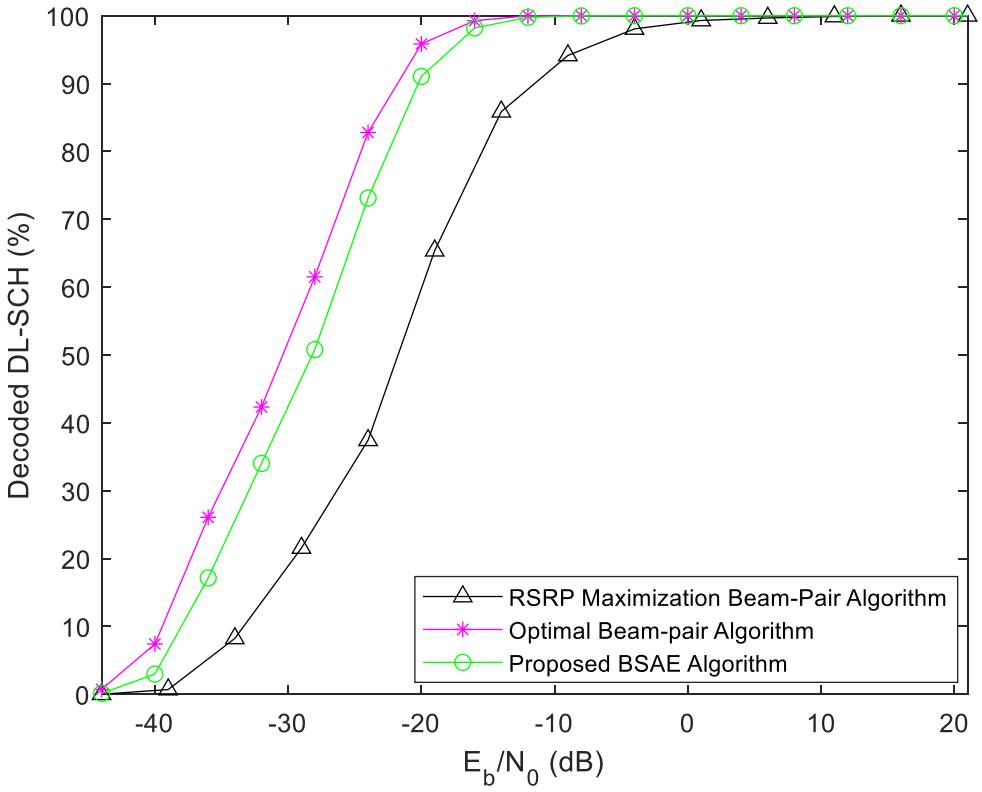

Figure 4.16: Decoding percentage of DL-SCH for FR1.

The respective performance results in terms of BER for the three algorithms mentioned above are presented in the following Figure 4.17, where the proposed BSAE algorithm presents a clear improvement over the beam-pair selection based on RSRP maximization algorithm, with a performance gain around 17.5 dB at BER target 10^{-3}.

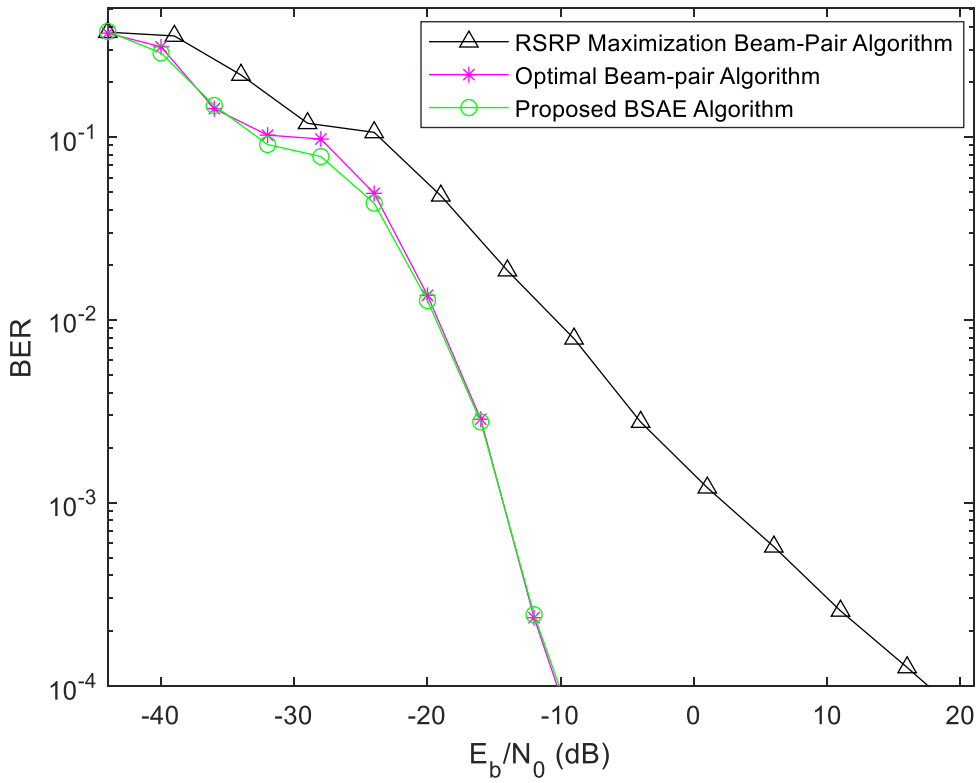

Figure 4.17: Performance BER comparison of the 3 different algorithms for FR1.

4.3.2 FR2 operation mode

In a similar way to the previous presented results, the following Figure 4.18 to Figure 4.20 illustrate the comparison of the different decoding percentages of the DL PHY channels of the three algorithms referred above for the FR2 operation mode. We can verify an enhancement of the designed BSAE algorithm for all the channel decoding percentages against the performance of the beam-pair selection algorithm based on RSRP maximization. Additionally, the BSAE algorithm achieves sensibly 100% throughput percentage for values higher than E_b / N_0= -24 dB, which corresponds to a sensibly 4 dB performance improvement gain. Comparing the decoding throughputs between the proposed and an optimal beam pair determination algorithms, it is still possible to observe similar performances.

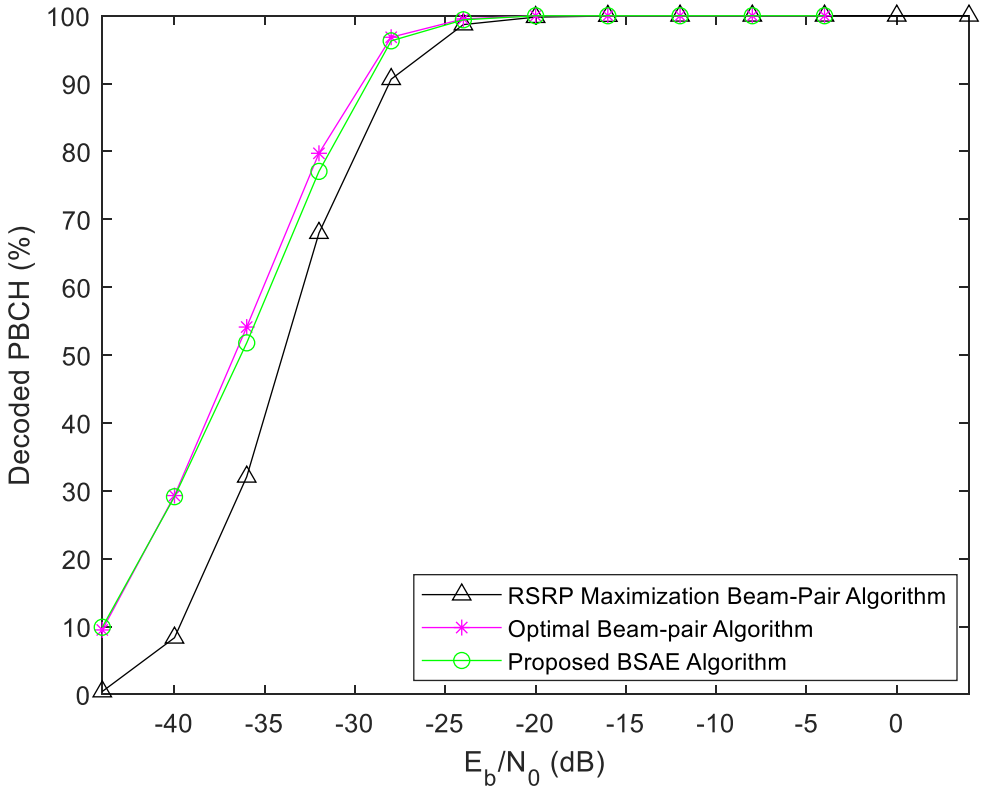

Figure 4.18: Decoding percentage of PBCH for FR2.

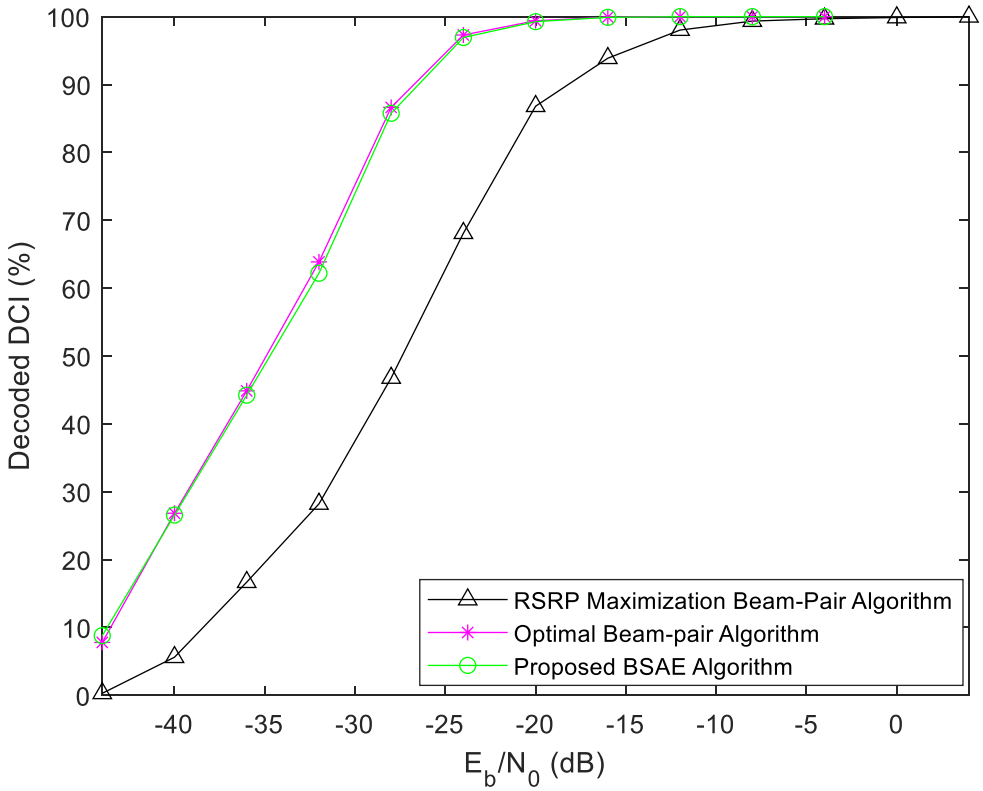

Figure 4.19: Decoding percentage of PDCCH for FR2.

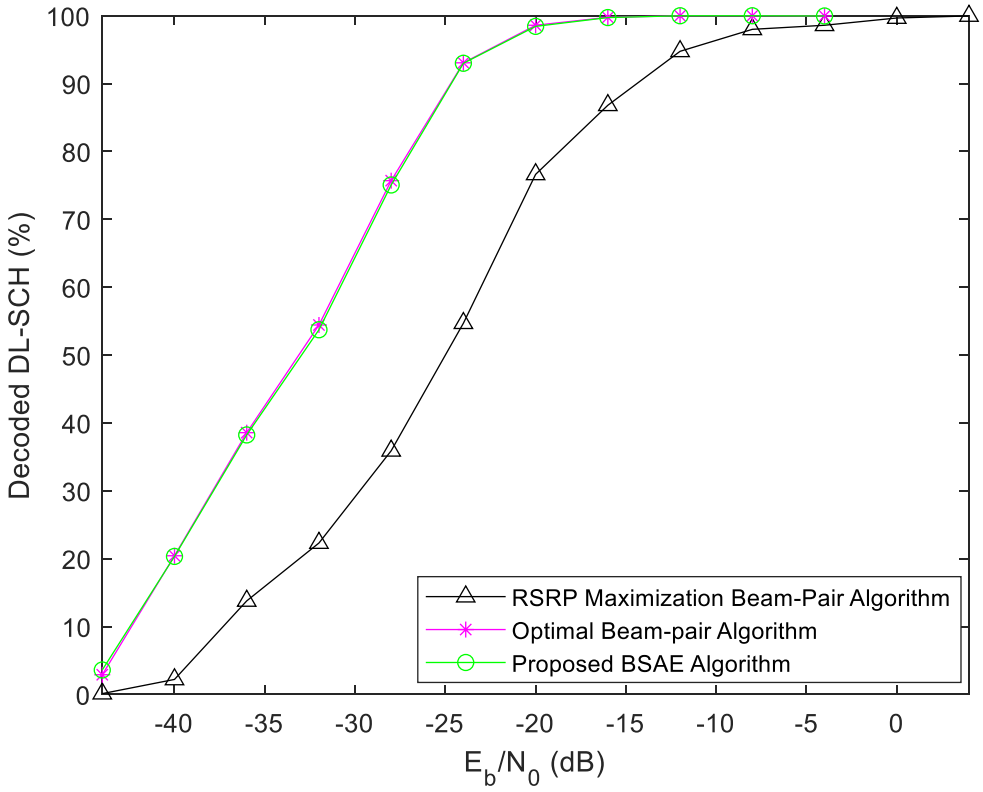

Figure 4.20: Decoding percentage of DL-SCH for FR2.

The respective performance results in terms of BER for the three algorithms mentioned above are presented in the following Figure 4.21, where the proposed BSAE algorithm presents a clear improvement over the beam-pair selection based on RSRP maximization algorithm, with a performance gain around 15 dB at BER target 10^{-3}.

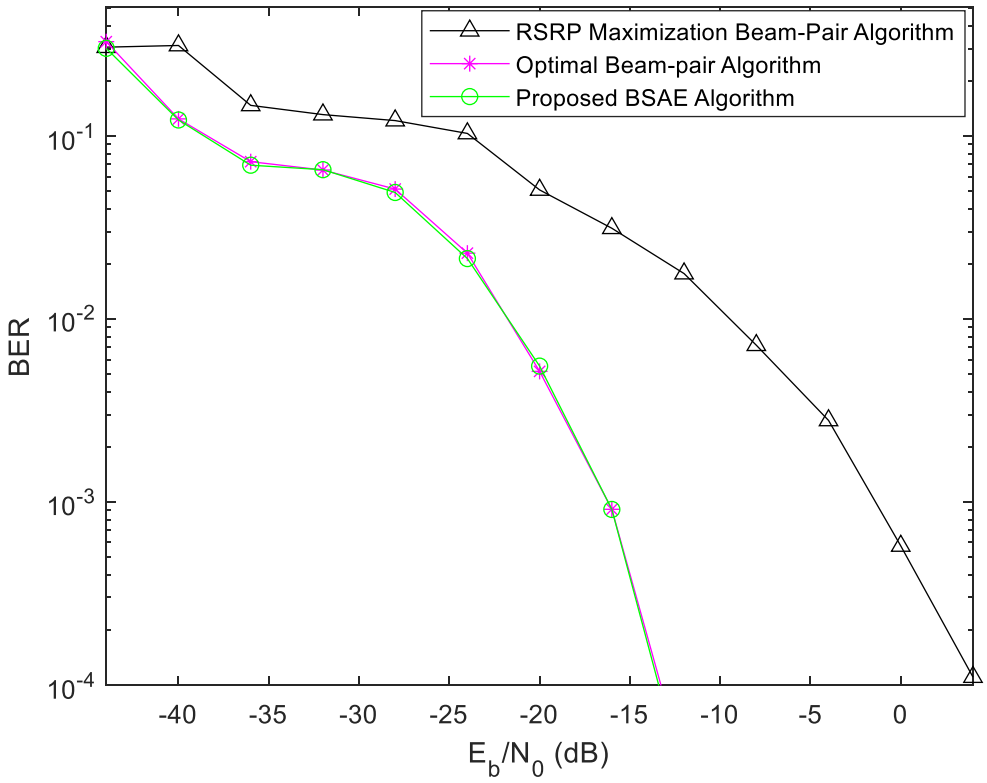

Figure 4.21: Performance BER comparison of the 3 different algorithms for FR2.

Chapter 5

5. Conclusions and Future Work

In this final chapter, the main conclusions are presented alongside some guidelines for future research and possible improvements.

5.1 Conclusions

The 3GPP organization has been constantly evolving through different generations of mobile communication systems, maintaining, and developing both new technical reports and specifications for more evolved technologies since the 3G networks. To answer the currently increase in the number of users in an already congested saturated spectrum, as well as their growing demands for the new wide range of possibilities and services on the edge to be enabled by future mobile communications, the 5G NR technology is being developed by 3GPP, combining the use of smaller cells in the so-called mmWave frequencies, characterized by stronger propagation losses. For an effective support of the mmWave higher frequencies, detailed control of both phase adjustments and amplitude scaling of the different antenna elements is needed, enabling BF techniques capable of producing precise directional transmission links over multiple receive and transmit antennas, overcoming the severe high path losses of mmWave systems. This led to the creation of a distinct set of PHY L1/L2 procedures known as BM procedures that specify how the suitable beamformed beam-pair links (a beam used at gNB paired with a beam used at the UE) are determined and maintained for transmission and reception of information in both DL and UL directions. The work developed in this dissertation addresses the guidelines on BF for 5G NR, providing a more detailed description of the BM procedures used during IA, applying, and evaluating them in a 3GPP-standard compliant implementation proposal involving the establishment of the best beam-pair link for further synchronization, demodulation and decoding of a live gNB signal.

Firstly, some important key enabler technologies and techniques used in the 5G NR systems to overcome the limited BW shortage of the LTE systems were presented. Here, the main features of the OFDM highly spectral-efficient modulation technique are discussed alongside the conventional MIMO systems adopted in LTE technology, used to improve the overall system performance taking advantage of multiple antennas terminals to provide multiplexing and diversity gains. These two technologies can be used together, presenting an effective combination capable of mitigating the multipath propagation effects while avoiding the need for complex channel equalization since all the OFDM subcarriers are orthogonal to each other, greatly reducing the ISI in both time and frequency domains. Thus, MIMO-OFDM systems enable good spectral efficiency and therefore, deliver high data throughput and capacity. Next, the mmWave propagation characteristics and challenges were revised together with their implementation with mMIMO systems, combining the use of much

smaller wavelengths of the mmWave frequencies to allow the implementation of a higher number of antenna elements in the same needed physical space compared to the 4G microwave communication systems. The conjugation of these two technologies is used to achieve the 3GPP requirements of increased capacity and data rates both in SA and NSA modes, enabling the employment of more sophisticated spatial processing techniques, such as BF in mMIMO systems, capable of compensating the propagation loses associated to the mmWaves systems and providing transmissions with reduced multi-user interference. After, an overview of the NR radio access technology is described, including some basic design principles, a brief description of the overall NR radio access architecture with the associated 5GC, and the most important technology concepts for a better comprehension of the BM procedures applied for an efficient establishment and management of suitable beam-pairs. In here, the PHY layer is particularly focused, with a more detailed description of both physical channels and signals used in the DL direction, including their correspondent functions and contextualization.

Then, in chapter 3, the P1-BM procedures applied for IBE purposes in the DL direction at PHY and RRC layers are described according to information collected from multiple 3GPP technical releases and specifications documents, where beam sweeping, measurement, determination and reporting processes are performed to acquire initial cell synchronization, enabling UE measurements on the different TX beams with the purpose of establishing an initial beam-pair selection between the gNB and the UE. The IBE stage is the first of the three BM procedures by which beamformed connectivity is established and retained, consisting of PLMN selection, IA and RRC connection establishment. After the UE has selected a PLMN, the beam sweeping technique is performed at both gNB and UE sides, where each SSB of the transmitted burst is used to obtain DL synchronization and the respective RSRP beam measurements needed to an effective determination of the most appropriate beam-pair. The next step is known as beam reporting and corresponds to the second stage of IA, where the UE sends a PRACH request to the gNB with the necessary beam quality and beam decision information it needs to establish the connection. If this request is successful, the gNB will exchange additional SI at RRC connection establishment and the UE specific BF connection occurs with the switching from wide beam coverage to a more specific beam-centric coverage associated to narrower beam provided from beam refinement procedures.

Next, in chapter 4, a 3GPP standard compliant implementation of a NR system performing beam-pair determination based on RSRP maximization algorithm for subsequent decoding of the transmitted signal is compared to a more efficient designed beam-pair selection algorithm using channel estimation based on SSSs. A testing environment was created using for different scenarios and configurations, where BM procedures for idle users during IA were focused. The system consists of a NR SS Burst generation with the employment of beam sweeping techniques at both the TX and RX ends to beamform each SSB within the burst over both azimuth and elevation directions through a spatial scattering channel for subsequent RX signal processing over the multiple receive-end beams. After the performed RSRP measurements for each of the transmit-receive beam-pairs, the one with the maximum RSRP value is chosen as the most suitable beam-pair for the simulated spatial scenario and then the UE performs cell selection procedures to obtain the initial SI needed to establish the SFN, the PCI and the MIB. These last procedures deliver all the necessary information for the

blind decoding of the DCI in the PDCCH, which will be further used for PDSCH configuration, decoding of the DL-SCH and to finally recover the SIB1 for every simulated symbol.

Finally, it can be concluded that the design and employment of efficient algorithms that explore BM procedures for beam-pair selection is of extreme importance and carries a significant impact in the overall system performance. The obtained results for the designed BSAE algorithm showed a considerable performance improvement over the beam pair determination algorithm based on RSRP maximization without the addition of much complexity. This emphasizes the benefits of designing algorithms that consider information about all the candidate beam pairs for an effective enhanced beam pair selection between the gNB and the UE. Additionally, when comparing the results between the proposed BSAE algorithm and the optimal case, similar performances are also noticeable, highlighting its potential for practical 5G mmWave mMIMO implementations following 3GPP-compliant standards.

5.2 Future Work

In this subchapter, some guidelines for future work are presented. Future efforts include:

- Simulation upon other numerology configurations with different SCSs and different SSB patterns that optimize the beam-pair selection with channel estimation techniques for different scenarios.

- Implementation and performance comparisons of higher order 64-QAM and 256-QAM modulation schemes intended for 5G.

- Extension to massive-MIMO hybrid architectures and subsequent trade-offs between complexity and performance.

- Real-time implementation of the work delivered in this dissertation.

References

[1] M. L. Roberts, M. A. Temple, R. F. Mills and R. A. Raines, "Evolution of the air interface of cellular communications systems toward 4G realization," *IEEE Communications Surveys & Tutorials,* vol. 8, no. 1, pp. 2-23, 2006.

[2] E. Dahlman, S. Parkvall and J. Sköld, 5G NR: The Next Generation Wireless Access Technology, 2018.

[3] B. A. Kumar and P. T. Rao, "Overview of advances in communication technologies," *2015 13th International Conference on Electromagnetic Interference and Compatibility (INCEMIC),* pp. 22-23, July 2015.

[4] Ericsson, "Ericsson Mobility Report," June 2021. [Online]. Available: https://www.ericsson.com/4a03c2/assets/local/reports-papers/mobility-report/documents/2021/june-2021-ericsson-mobility-report.pdf.

[5] J. D. Vriendt, P. Laine, C. Lerouge and X. Xu, "Mobile network evolution: a revolution on the move," *IEEE Communications Magazine,* vol. 40, no. 4, pp. 104-111, April 2002.

[6] P. Rost, A. Banchs, I. Berberana, M. Breitbach, M. Doll, H. Droste, C. Mannweiler, M. A. Puente, K. Samdanis and B. Sayadi, "Mobile network architecture evolution toward 5G," *IEEE Communications Magazine,* vol. 54, no. 5, pp. 84-91, May 2016.

[7] V. K. Garg, S. Halpern and K. F. Smolik, "Third generation (3G) mobile communications systems," in *1999 IEEE International Conference on Personal Wireless Communications*, Jaipur, India, 1999.

[8] M. R. Bhalla and A. V. Bhalla, "Generations of Mobille Wireless Technology: A Survey," *International Journal of Computer Applications,* vol. 5, no. 4, pp. 26-32, August 2010.

[9] R. C. Qiu, W. Zhu and Y.-Q. Zhang, "Third-generation and beyond (3.5G) wireless networks and its applications," *2002 IEEE International Symposium on Circuits and Systems (ISCAS),* pp. 26-29, August 2002.

[10] H. Ekstrom, A. Furuskar, J. Karlsson, M. Meyer, S. Parkvall, J. Torsner and M. Wahlqvist, "Technical solutions for the 3G long-term evolution," *IEEE Communications Magazine,* vol. 44, no. 3, pp. 38-45, March 2006.

[11] A. Ghosh, W. Xiao, R. Ratasuk, A. Rottinghaus and B. Classon, "Multi-antenna system design for 3GPP LTE," *2008 IEEE International Symposium on Wireless Communication Systems,* December 2008.

[12] D. Astely, E. Dahlman, A. Furuskär, Y. Jading, M. Lindström and S. Parkvall, "LTE: the evolution of mobile broadband," *IEEE Communications Magazine,* vol. 47, no. 4, pp. 44-51, April 2009.

[13] 3GPP, "Evolved Universal Tereestrial Radio Access (E-UTRA); Requirements for support of radio resource management," *TS 36.133 V17.6.0,* June 2022.

[14] Qualcomm, "The Evolution of Mobile Technologies: 1G - 2G - 3G - 4G LTE," [Online]. Available: https://www.qualcomm.com/content/dam/qcomm-martech/dm-assets/documents/the_evolution_of_mobile_technologies-wireless-networks.pdf.

[15] 3GPP, "Massive Internet of Things," *TR 22.861 V14.1.0,* September 2016.

[16] L. Chettri and R. Bera, "A Comprehensive Survey on Interneet of Things (IoT) Toward 5G Wireless Systems," *IEEE Internet of Things Journal,* vol. 7, no. 1, pp. 16-32, January 2020.

[17] ITU-R, "IMT Vision- Framework and overall objectives of the future development of IMT for 2020 and beyond," *M Series 2083-0,* September 2015.

[18] E. Dahlman, G. Mildh, S. Parkvall, J. Peisa, J. Sachs, Y. Selén and J. Sköld, "5G wireless access: requirements and realization," *IEEE Communications Magazine,* vol. 52, no. 12, pp. 42-47, December 2014.

[19] 3GPP, "Feasibility study on new services and markets technology enablers for enhanced mobile broadband; Stage 1," *TR 22.863 V14.1.0,* September 2016.

[20] 3GPP, "Service requirements for Machine-Type Communications (MTC); Stage 1," *TS 22.368 V17.0.0 ,* April 2022.

[21] 3GPP, "Feasibility study on new services and markets technology enablers for critical communications; Stage 1," *TR 22.862 V14.1.0,* October 2016.

[22] M. Carugi, "Key features and requirements of 5G/IMT-2020 networks," [Online]. Available: https://www.itu.int/en/ITU-D/Regional-Presence/ArabStates/Documents/events/2018/RDF/Workshop%20Presentations/Session1/5G-%20IMT2020-presentation-Marco-Carugi-final-reduced.pdf.

[23] S. Parkvall, Y. Blankenship, R. Blasco, E. Dahlman, G. Fodor, S. Grant, E. Stare and M. Stattin, "5G NR Realease 16: Start of the 5G Evolution," *IEEE Communications Standards Magazine,* vol. 4, no. 4, pp. 56-63, December 2020.

[24] 3GPP, "Release 17 Description; Summary ofRel-17 Work Items," *TR 21.917 V1.0.0,* September 2022.

[25] I. Rahman, S. M. Razavi, O. Liberg, C. Hoymann, H. Wiemann, C. Tidestav, P. Schliwa-Bertling, P. Persson and D. Gerstenberger, "5G Evolution Toward 5G Advanced: An Overview of 3GPP releases 17 and 18," [Online]. Available: https://www.ericsson.com/4a92c5/assets/local/reports-papers/ericsson-technology-review/docs/2021/an-overview-of-3gpp-releases-17-and-18.pdf.

[26] ITU-R, "Detailed specifications of the terrestrial radio interfaces of International Mobile Tellecomunications-2020 (IMT-2020)," *Recommendation ITU-R M.2150-1,* February 2022.

[27] I. Hemadeh, M. El-Hajjar, S. Katla and L. Hanzo, "Millimeter-Wave Communications: Physical Channel Models, Design Considerations, Antenna Constructions and Link-Budget," in *IEEE Communications Surveys & Tutorials*, 2017.

[28] E. G. Larsson, O. Edfors, F. Tufvesson and T. L. Marzetta, "Massive MIMO for next generation wireless systems," *IEEE Communications Magazine,* vol. 52, no. 2, pp. 186-195, February 2014.

[29] 3GPP, "Study on New Radio Access Technology Physical layer aspects," *TR 38.802 V14.2.0*, September 2017.

[30] M. Giordani, M. Mezzavilla, C. N. Barati, S. Rangan and M. Zorzi, "Comparative analisys of initial access techniques in 5G mmWave cellular networks," in *2016 Annual Conference on Information Science and Systems (CISS)*, Princeton.

[31] R. Baldemair, E. Dahlman, G. Fodor, G. Mildh, S. Parkvall, Y. Selen, H. Tullberg and K. Balachandran, "Evolving Wireless Communications: Addressing the Challenges and Expectations of the Future," *IEEE Vehicular Technology Magazine*, vol. 8, no. 1, pp. 24-30, March 2013.

[32] Y. Xiao, S. Wang, L. Dan, X. Lei, P. Yang and W. Xiang, "OFDM with Interleaved Subcarrier-Index Modulation," *IEEE Communications Letters*, vol. 18, no. 8, pp. 1447-1450, August 2014.

[33] A. R. S. Bahai, B. R. Saltzberg and M. Ergen, Multi-Carrier Digital Communications: Theory and Applications of OFDM, Second ed., Springer Science & Business Media, 1999, p. 411.

[34] "Concepts of Orthogonal Frequency Division Multiplexing (OFDM) and 802.11 WLAN," [Online]. Available: https://rfmw.em.keysight.com/wireless/helpfiles/89600b/webhelp/subsystems/wlan-ofdm/content/ofdm_basicprinciplesoverview.htm.

[35] J. Li, K. B. Letaief and Z. Cao, "Co-channel interference cancellation for space-time coded OFDM systems," *IEEE Transactions on Wireless Communications*, vol. 2, no. 1, pp. 41-49, January 2003.

[36] X. Wang, P. Ho and Y. Wu, "Robust channel estimation and ISI cancellation for OFDM systems with suppressed features," *IEEE Journal on Selected Areas in Communications*, vol. 235, pp. 963-972, May 2005.

[37] C. Sturm, T. Zwick and W. Wiesbeck, "An OFDM System Concept for Joint Radar and Communications Operations," in *VTC Spring 2009 - IEEE 69th Vehicular Technology Conference*, Barcelona, 2009.

[38] P. Banelli, S. Buzzi, G. Colavolpe, A. Modenini, F. Rusek and A. Ugolini, "Modulation Formats and Waveforms for 5G Networks: Who Will Be the Heir of OFDM? An overview of alternative modulation schemes for improved spectral efficiency," *IEEE Signal Processing Magazine*, vol. 31, no. 6, pp. 80-93, November 2014.

[39] A. Goldsmith, S. A. Jafar, N. Jindal and S. Vishwanath, "Capacity limits of MIMO channels," *IEEE Journal on Selected Areas in Communications*, vol. 21, no. 5, pp. 684-702, June 2003.

[40] S. Sanayei and A. Nosratinia, "Antenna selection in MIMO systems," *IEEE Communications Magazine*, vol. 42, no. 10, pp. 68-73, October 2004.

[41] J. Mietzner, R. Schober, L. Lampe, W. H. Gerstacker and P. A. Hoeher, "Multiple-antenna techniques for wireless communications - a comprehensive literature survey," *IEEE Communications Surveys & Tutorials*, vol. 11, no. 2, pp. 87-105, June 2009.

[42] C. Johnson, 5G New Radio in Bullets, 1 ed., 2019.

[43] F. Khan and Z. Pi, "mmWave mobile broadband (MMB): Unleashing the 3-300GHz spectrum," in *34th IEEE Sarnoff Symposium*, Princetown, NJ, USA, 2011.

[44] T. S.Rappaport, S. Sun, R. Mayzus, H. Zhao, Y. Azar, K. Wang, G. N. Wong, J. K. Schulz, M. Samimi and F. Gutierrez, "Millimeter Wave Mobile Communications for 5G Cellular: It Will Work!," *IEEE Access*, vol. 1, pp. 335-349, May 2013.

[45] Z. Pi and F. Khan, "An introduction to millimeter-wave mobile broadband systems," *IEEE Communications Magazine*, vol. 49, no. 6, pp. 101-107, June 2011.

[46] W. Roh, J.-Y. Seol, J. Park, B. Lee, J. Lee, Y. Kim, J. Cho, K. Cheun and F. Aryanfar, "Millimeter-Wave Beamforming as an enabling Technology for 5G Cellular Communications: Theoretical Feseability and Prototype Results," *Communications Magazine, IEEE*, vol. 52, no. 2, pp. 106-113, February 2014.

[47] S. Ahmadi, 5G NR: Architecture, Technology, Implementation, and Operation of 3GPP New Radio Satndards, 2019.

[48] S. Hur, T. Kim, D. J. Love, J. V. Krogmeier, T. A. Thomas and A. Ghosh, "Millimeter Wave Beamforming for Wireless Backhaul and Access in Small Cell Networks," *IEEE Transactions on Communications*, vol. 61, no. 10, pp. 2-13, June 2013.

[49] 3GPP, "NR and NG-RAN Overall description; Stage-2," *TS 38.300 V17.1.0*, July 2022.

[50] 3GPP, "Study on new radio access technology: Radio access architecture and interfaces," *TR 38.801 V14.0.0*, April 2017.

[51] 3GPP, "System Architecture for the 5G System (5GS)," *TS 23.501 V17.5.0*, June 2022.

[52] 3GPP, "NG-RAN; Architecture description," *TS 38.401 V17.1.1*, July 2022.

[53] 3GPP, "NG-RAN; NR user plane protocol," *TS 38.425 V17.0.0*, April 2022.

[54] 3GPP, "NR; Radio Resource Control (RRC); Protocol specification," *TS 38.331 V17.1.0*, July 2022.

[55] 3GPP, "NR; Physical channels and modulation," *TS 38.211 V17.2.0*, June 2022.

[56] 3GPP, "Study on New Radio (NR) access technology," *TR 38.912 V17.0.0*, April 2022.

[57] A. A. Zaidi, R. Baldemair, V. Moles-Cases, N. He, K. Werner and A. Cedergren, "OFDM Numerology Design for 5G New Radio to Support IoT, eMBB, and MBSFN," *IEEE Communications Standards Magazine*, vol. 2, no. 2, pp. 78-83, June 2018.

[58] S. Teodoro, A. Silva, R. Dinis, F. M. Barradas, P. M. Cabral and A. Gameiro, "Theoretical Analysis of Nonlinear Amplification Effects in Massive MIMO Systems," pp. 1-3, December 2019.

[59] A. Ghosh, A. Maeder, M. Baker and D. Chandramouli, "5G Evolution: A View on 5G CellularTechnology Beyond 3GPP Release 15," *IEEE Access*, vol. 7, September 2019.

[60] P. Guan, D. Wu, T. Tian, J. Zhou, X. Zhang, L. Gu, A. Benjebbour, M. Iwabuchi and Y. Kishiyama, "5G Field Trials: OFDM-Based Waveforms and Mixed Numerologies," *IEEE Journal on Selected Areas in Communications*, vol. 35, no. 6, pp. 1234-1243, June 2017.

[61] X. Zhang, L. Zhang, P. Xiao, D. Ma, J. Wei and Y. Xin, "Mixed Numerologies Interference Analysis and Inter-Numerology Interference Cancellation for Windowed OFDM Systems," *IEEE Transactions on Vehicular Technology,* vol. 67, no. 8, August 2018.

[62] 3GPP, "NR; Base Station (BS) radio transmission and reception," *TS 38.104 V17.6.0,* June 2022.

[63] A. Kumar. [Online]. Available: https://cafetele.com/bwp/.

[64] 3GPP, "NR; Physical layer procedures for control," *TS 38.213 V17.2.0,* June 2022.

[65] 3GPP, "NR; User Equipment (UE) radio transmission and reception; Part 2: Range 2," *TS 38.101-2 V17.6.0,* June 2022.

[66] 3GPP, "NR; User Equipment (UE) procedures in idle mode and in RRC Inactive state," *TS 38.304 V17.1.0,* July 2022.

[67] Y.-N. R. Li, M. Chen, J. Xu, L. Tian and K. Huang, "Power Saving Techniques for 5G and Beyond," *IEEE Access,* vol. 8, June 2020.

[68] sharetechnote, "5G/NR - SS Block," [Online]. Available: https://www.sharetechnote.com/html/5G/5G_SS_Block.html.

[69] "5G/NR - Beam Management," [Online]. Available: https://www.sharetechnote.com/html/5G/5G_Phy_BeamManagement.html.

[70] MATLAB, "NR SSB Beam Sweeping," [Online]. Available: https://www.mathworks.com/help/5g/ug/nr-ssb-beam-sweeping.html.

[71] H. Yang, A. Huang, R. Gao, T. Chang and L. Xie, "Interference Self-Coordination: a Proposal to Enhance Reliability of System-Level Information in OFDM-Based Mobile Networks via PCI Planning," *IEEE Transactions on Wireless Communications,* vol. 13, no. 4, pp. 1874-1887, April 2014.

[72] C. N. Barati, S. A. Hosseini, S. Rangan, P. Liu, T. Korakis, S. S. Panwar and T. S. Rappaport, "Directional Cell Discovery in Millimeter Wave Cellular Networks," *IEEE Transactions on Wireless Communications,* vol. 14, no. 12, pp. 6664-6678, December 2015.

[73] C. N. Barati, S. A. Hosseini, M. Mezzavilla, T. Korakis, S. S. Panwar, S. Rangan and M. Zorzi, "Initial Access in Millimeter Wave Cellular Systems," *IEEE Transactions on Wireless Communications,* vol. 15, no. 12, pp. 7926-7940, December 2016.

[74] T. Nitsche, A. B. Flores, E. W. Knightly and J. Widmer, "Steering with eyes closed: Mm-Wave beam steering without in-band measurement," in *2015 IEEE Conference on Computer Communications (INFOCOM),* Hong Kong, 2015.

[75] V. Desai, L. Krzymien, P. Sartori, W. Xiao, A. Soong and A. Alkhateeb, "Initial beamforming for mmWave communications," in *2014 48th Asilomar Conference on Signals, Systems and Computers*, Pacific Grove, CA, 2014.

[76] L. Wei, Q. Li and G. Wu, "Exhaustive, Iterative and Hybrid Inital Access Techniques in mmWave Communications," in *2017 IEEE Wireless Communications and Networking Conference (WCNC),* San Francisco, CA, 2017.

[77] A. Ali, N. González-Prelcic and R. W. Heath, "Millimeter Wave BEam-Selection Using Out-of-Band Spatial Information," *IEEE Transactions on Wireless Communications*, vol. 17, no. 2, pp. 1038-1052, February 2018.

[78] V. Va, T. Shimizu, G. Bansal and R. W. Heath, "Position-aided millimeter Wave V2I beam alignment: A learning-to-rank approach," in *2017 IEEE 28th Annual International Symposium on Personal, Indoor, and Mobile Radio Communications*, Montreal, QC, 2017.

[79] W. Xu, F. Gao, S. Jin and A. Alkhateeb, "3D Scene-Based Beam Selection for mmWave Communications," *IEEE Wireless Communications Letters*, vol. 9, no. 11, pp. 1850-1854, November 2020.

[80] A. Ali, J. Mo, B. L. Ng, V. Va and J. C. Zhang, "Orientation-Assisted Beam Management for Beyond 5G Systems," *IEEE Access*, vol. 9, pp. 51832-51846, March 2021.

[81] Mathworks, "phased.ScatteringMIMOChannel," [Online]. Available: https://www.mathworks.com/help/phased/ref/phased.scatteringmimochannel-system-object.html.

[82] Mathworks, "NR Cell Search and MIB and SIB1 Recovery," [Online]. Available: https://www.mathworks.com/help/5g/ug/nr-cell-search-and-mib-and-sib1-recovery.html.

[83] 3GPP, "Study on 3D channel model for LTE," *TR 36.873 V12.7.0,* January 2018.

[84] 3GPP, "Study on channel model for frequency spectrum above 6GHz," *TR 38.900 V15.0.0,* June 2018.

[85] 3GPP, "User Equipment (UE) radio transmission and reception; Part1: Range 1," *TS 38.101-1 V17.6.0,* June 2022.

[86] 3GPP, "User Equipment (UE) radio transmission and reception; Part 2: Range 2," *TS 38.101-2 V17.6.0,* June 2022.

[87] 3GPP, "User Equipment (UE) radio transmission and reception; Part 3: Range 1 and Range 2 Interworking operation with other radios," *TS 38.101-3 V17.6.0,* June 2022.

[88] 3GPP, "NR; Physical layer procedures for data," *TS 38.214 V17.2.0 ,* June 2022.

[89] 3GPP, "NR; Requirements for support of radio resource management," *TS 38.133 V17.6,* June 2022.

[90] 3GPP, "NR; Multiplexing and channel coding," *TS 38.212 V17.2.0 ,* June 2022.

[91] 3GPP, "NR; User Equipment (UE) radio access capabilities," *TS 38.306 V17.1.0,* July 2022.

[92] 3GPP, "Study of Radio Frequency (RF) and Electromagnetic Compatibility (EMC) requirements for Active Antenna Array System (AAS) base station," *TR 37.840 V12.1.0,* January 2014.

[93] J. Smee, "5 key technology inventions in 5G NR Release 17," [Online]. Available: https://www.rcrwireless.com/20220414/5g/5-key-technology-inventions-in-5g-nr-release-17.